Slow slip events in Mexico revised from the processing of 11 year GPS observations

M. Vergnolle, A. Walpersdorf, V. Kostoglodov, P. Tregoning, J. A. Santiago, N. Cotte, S. I. Franco

Slow slip events in Mexico revised from the processing of 11 year GPS observations

M. Vergnolle,[1,2] A. Walpersdorf,[1] V. Kostoglodov,[3] P. Tregoning,[4] J. A. Santiago,[3] N. Cotte,[1] and S. I. Franco[5]

Received 5 August 2009; revised 15 February 2010; accepted 25 February 2010; published 7 August 2010.

[1] The world's largest observed Slow Slip Events (SSE) occurred in 2001–2002 and 2006 in the Guerrero subduction zone, Mexico. Using an improved GPS processing that accounts for time-varying atmospheric phenomena as well as oceanic, atmospheric and hydrologic loading corrections, the 11 year GPS position time series in Guerrero show a noise reduction of ~50% with respect to previous studies. Thanks to the improved position time series and, in particular, the simultaneous analysis of the three-dimensional GPS observations, we can provide new information about SSEs in the studied area. First, we detect seven nonperiodic anomalous displacements with subcentimeter amplitude, but no quasi-annual anomalies as proposed previously. The displacements seem to occur simultaneously with the observed peaks of non-volcanic tremor activity in the area. Second, we refine the characteristics of the two major SSEs in terms of timing, duration, and cumulative displacements, and highlight the complex surface spatiotemporal evolution of the displacements during these SSEs. In particular, we observe a clear initiation phase for the 2006 SSE as well as ending phases for both large SSEs. The ending phase shows a strong deceleration of the anomalous displacements with respect to the main displacement phase already observed, for the 2001–2002 and 2006 SSEs. The duration of the SSEs increases by 30–40% including the initiation and ending phases. For the 2006 SSE, the main displacement phase also shows spatiotemporal complexity. Our results demonstrate the need for improved three-dimensional GPS processing technique in order to undertake detailed studies of SSEs.

Citation: Vergnolle, M., A. Walpersdorf, V. Kostoglodov, P. Tregoning, J. A. Santiago, N. Cotte, and S. I. Franco (2010), Slow slip events in Mexico revised from the processing of 11 year GPS observations, *J. Geophys. Res.*, *115*, B08403, doi:10.1029/2009JB006852.

1. Introduction

[2] Recent observations of aseismic slow slip events (SSEs), made in most of the geodetically well instrumented subduction zones [*Schwartz and Rokosky*, 2007, and references therein], demonstrate that the loading process during the interseismic period is not uniform and with a constant rate as had been assumed [*Reid*, 1910]. This discovery changes our concept of the recurrence of large earthquakes. Precise knowledge of SSEs characteristics is a prerequisite to any deeper understanding of the loading and releasing process on faults and thus on earthquake cycles. SSEs have been discovered in the Pacific subduction zones: Cascadia [e.g., *Dragert et al.*, 2001; *Miller et al.*, 2002; *Szeliga et al.*, 2004], Japan [e.g., *Hirose et al.*, 1999; *Ozawa et al.*, 2001], Mexico [e.g., *Lowry et al.*, 2001; *Kostoglodov et al.*, 2003; *Larson et al.*, 2007], Alaska [e.g., *Ohta et al.*, 2006], New Zealand [e.g., *Douglas et al.*, 2005] and Costa Rica [e.g., *Protti et al.*, 2004; *Brown et al.*, 2005]. SSEs have also been reported on strike-slip [e.g., *Linde et al.*, 1996; *Gwyther et al.*, 2000], and normal faults [*Doubre and Peltzer*, 2007]. It is thus possible that SSEs are a common feature of the interseismic loading of most faults.

[3] The documented SSEs that occur in subduction zones exhibit some similar characteristics. The slip rate is too slow to generate seismic radiation but is commonly faster than the interseismic loading rate. The surface displacements occur in a direction approximately opposite to, but somewhat oblique to, the steady loading direction. However, the SSEs also show large variations in duration (from days to years), in surface displacement amplitude (few millimeters to few centimeters) and in recurrence behavior (from no repetition at the observation time scale through episodic to periodic occurrence).

[1]Laboratoire de Géophysique Interne et Tectonophysique, CNRS, Observatoire de Grenoble, Université Joseph Fourier, Grenoble, France.
[2]Now at Géoazur, UMR6526, University of Nice, CNRS, Valbonne, France.
[3]Instituto de Geofísica, Universidad Nacional Autónoma de México, Mexico City, Mexico.
[4]Research School of Earth Sciences, Australian National University, Canberra, ACT, Australia.
[5]Servicio Sismológico Nacional, Instituto de Geofísica, Universidad Nacional Autónoma de México, Mexico City, Mexico.

0148-0227/10/2009JB006852

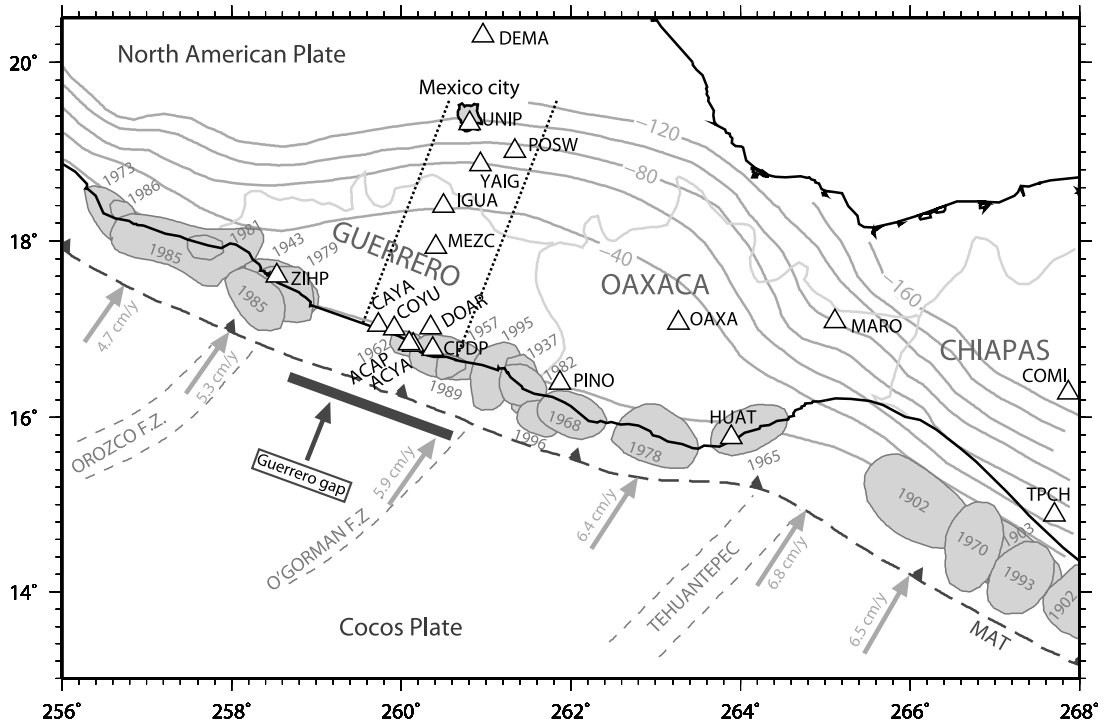

Figure 1. Seismotectonic map [after *Franco et al.*, 2005] and GPS station locations (white triangles). The arrows indicate the direction and magnitude of NUVEL1-A relative plate motion between the Cocos and North American plates [*DeMets et al.*, 1994]. The gray patches represent the major earthquake rupture zones. The gray lines and negative values (in km) indicate the slab iso-depths. The parallel dashed lines show the stations used in the dislocation model (section 6.2 and Figure 7).

[4] Under the assumption that the aseismic slip occurs on the subduction interface, most of the surface displacement inversions locate the SSEs at the downdip extension of the seismogenic zone except for the 1996 Boso and 2003 Costa Rica SSEs [*Sagiya*, 2004; *Protti et al.*, 2004] for which the aseismic slip could occur also in the lower or upper part of the seismogenic zone. These scenarios lead to different seismic hazard interpretations such as the advanced or delayed occurrence of the next subduction thrust earthquake [*Thatcher*, 2001] or the (effective) size reduction of the next earthquake [e.g., *Correa-Mora et al.*, 2008]. Hence, the precise determination of the location, amplitude and frequency of SSEs is of critical importance to evaluate their impact on the setting, size and occurrence of large subduction earthquakes and thus to evaluate the hazard level in these highly dangerous seismic regions.

[5] In order to contribute to this goal, we re-analyzed 11 years of GPS observations at the stations located in Guerrero, Mexico. Specifically, we aimed to reduce the processing and non-tectonic geophysical noise affecting the measurements (section 3 and Appendix A) to refine the primary key parameters (e.g., occurrence, surface displacement amplitude, spatiotemporal evolution) of the SSEs in this area. The new GPS position time series, and in particular, the simultaneous analysis of the three dimensional GPS observations enable us to revise the SSE characteristics, confirming the presence of only some of the small SSEs observed previously (section 4) and documenting the time evolution of the largest SSEs (section 5). We discuss these new observations (section 6) that provide new constraints for further investigations on the slip localization at depth, propagation and mechanism.

2. Guerrero Subduction Zone

[6] The Guerrero subduction segment is part of the Middle American Trench (MAT). It extends from 261°E to 258.4°E and encompasses the NW Guerrero gap - where no large subduction earthquake has occurred since 1911 (Ms 7.8) [*Ortiz et al.*, 2000] - and the SE Guerrero gap which overlaps the rupture lengths of the 1907 (Ms 7.9), 1957 (Mw 7.8) and 1962 (Mw 7.1 and Mw 7.0) earthquakes [*Ortiz et al.*, 2000; *Anderson et al.*, 1994] (Figure 1). According to *Suárez et al.* [1990] and *Anderson et al.* [1994], the total seismic moment of the moderate earthquakes in the 20th century is not sufficient to accommodate the expected strain accumulation in the Guerrero gap. This seismic gap could then rupture with an earthquake of magnitude as high as Mw 8.4. Both the convergence rate between the Cocos and the North American Plates along the MAT and the geometry of the subducting slab in Guerrero govern the subduction thrust earthquake process and the crustal deformation as distant as Mexico City. The slab interface dips down to ~40 km depth at a distance of ~140 km from the trench. At this depth the slab bends sharply and lies sub-horizontally beneath central Mexico [*Suárez et al.*, 1990; *Kostoglodov et al.*, 1996; *Pérez-Campos et al.*, 2008]. With this configuration, the seismogenic zone in Guerrero is supposed to be limited to 25 km depth [*Suárez et al.*, 1990]. The location of the locked zone

is confirmed by studies of seismicity [*Suárez et al.*, 1990; *Singh and Pardo*, 1993; *Pardo and Suárez*, 1995], and by inter-seismic deformation studies based on geodetic data [*Kostoglodov et al.*, 2001; *Larson et al.*, 2004].

[7] Since the installation of a permanent GPS network in the Guerrero area, several SSEs have been observed [*Lowry et al.*, 2001; *Kostoglodov et al.*, 2003; *Larson et al.*, 2004; *Franco et al.*, 2005; *Lowry*, 2006; *Larson et al.*, 2007]. Large SSEs that occurred in 1998, 2001–2002 and 2006 produced up to 5–6 cm of surface displacements and are some of the largest SSEs ever observed (equivalent magnitude of up to Mw 7.6). The SSEs crustal displacements affected a large area, up to 550 x 250 km^2 in 2001–2002 [*Iglesias et al.*, 2004]. The slip propagated from central Guerrero to the NW and SE along the coast at a rate of ~2 km/day for the 2001–2002 SSE [*Franco et al.*, 2005]. The slip was mainly in the transition zone but could have intruded into the seismogenic zone [*Yoshioka et al.*, 2004; *Iglesias et al.*, 2004; *Larson et al.*, 2007]. Both the 2001–2002 and 2006 SSEs had similar surface displacements, in particular at sites on the coast [*Larson et al.*, 2007], whereas the 1998 SSE was smaller and is only poorly resolved [*Lowry et al.*, 2001; *Larson et al.*, 2004].

[8] Small periodic SSEs in 1999, 2000, 2001, 2003 and 2004 were reported by *Lowry* [2006]. The measured surface displacements during these SSEs ranged from a few millimeters to 1–2 cm. Taking into account the five small SSEs and the three large SSEs, *Lowry* [2006] deduced an SSE occurrence periodicity of 12.0±0.3 months and suggested that they may be interpreted as the resonant response to climate-driven stress perturbation. However, annual periodicity is also prevalent in GPS position estimates due to atmospheric, hydrological and oceanic mass transfers [e.g., *Blewitt et al.*, 2001] and separating analysis errors from these seasonal variations is not straightforward [*Dong et al.*, 2002; *Penna and Stewart*, 2003; *Tregoning and Watson*, 2009]. Thus, inferring that the observed annual changes in the 'tectonic' position time series are climate-driven may not be correct but, if so, would have a critical impact on our knowledge of SSEs and on the driving physical forces of repeating SSEs.

3. GPS Analysis

[9] Measuring the cumulative displacements of the large Guerrero SSEs can be achieved with standard GPS analysis strategies, but precisely determining the initiation and end of the SSEs, as well as their precise temporal evolution, and the presence of the small Guerrero SSEs, requires implementing the most accurate analysis strategies. The Mexican continuous GPS data (Figure 1, Appendix A) have been processed using an improved "climatic and loading" GPS processing strategy. We derived daily position time series with the GAMIT-GLOBK software [*Herring et al.*, 2006] but accounted for time-varying atmospheric phenomena, oceanic, atmospheric and hydrologic loading corrections. The application of the new time-varying atmospheric delay models and atmospheric loading corrections are still not used routinely in GPS analysis for active tectonic studies, while a posteriori hydrologic loading correction applied to the resulting position time series is currently very rare in GPS analysis and has only been used in methodological geodetic studies that aimed to reduce the noise (i.e., signals that are not tectonic signal) in the GPS position estimates. This work is currently the first attempt to integrate this correction in a regional GPS analysis focused on the observation of tectonic geophysical phenomena.

3.1. GPS Processing Strategy and Results

[10] Knowledge of the loading effects, which affect GPS position estimates, has greatly improved in the last few years [*Blewitt et al.*, 2001; *van Dam et al.*, 2001; *Tregoning et al.*, 2009] as well as the development of time-varying models of surface pressure and temperature [*Boehm et al.*, 2007b] and tropospheric mapping functions [*Boehm and Schuh*, 2004; *Boehm et al.*, 2006a, 2006b]. Considerable reductions of noise in GPS position estimates can be achieved by using these more sophisticated, time-varying representations of the atmosphere [e.g., *Steigenberger et al.*, 2009; *Tregoning and Watson*, 2009].

[11] Three strategies have been applied to the GPS data to establish the real improvement in using a more sophisticated processing approach. The description of these strategies, from a standard strategy (ST1) to a "first climatic and loading" strategy (ST2) to the "final climatic and loading" strategy (ST3, including a posteriori hydrologic loading correction) is presented in Table 1. The details of the GPS strategies are given in the Appendix A.

[12] To investigate the improvement in signal-to-noise ratio between the successive ST1, ST2 and ST3 strategies, we performed a residual analysis on the 3 components at all stations with more than 2 years of data during the "linear" inter-large-SSEs period assumed to be free of large SSEs (i.e., between 2003.0 and 2006.0). Twelve of 16 stations in the Guerrero area meet this criterion. We based our analysis on the number of stations for which the weighted root mean square (wrms) improved from one strategy to the next, as well as on the mean value of the improvement over all stations considered (δ, equation (1)).

$$\delta = \frac{\sum_{i=1}^{N} \frac{wrms_{STj,i} - wrms_{STk,i}}{wrms_{STj,i}}}{N} \times 100, \quad (1)$$

where *STj* is ST1 or ST2, *STk* is ST2 or ST3 respectively and *i* the stations. The improvement on each component from one strategy to the other is given in Table A1 and detailed in Appendix A. In particular, a comprehensive discussion about the impact of hydrological loading correction on the position estimates is presented in Appendix A and Figure A2. In summary, the repeatability of the position time series derived from the standard strategy (ST1, Table 1) and the "final climatic and loading" strategy (ST3, Table 1) improves by ~5 to ~30%. Hence, the use of the up-to-date and time varying mapping function and pressure models, and the application of atmospheric and hydrological loading corrections in a regional study yield significant improvements in the accuracy of coordinates estimates as already shown in global studies [*Tregoning and Herring*, 2006; *Boehm et al.*, 2007a; *Tregoning and van Dam*, 2005; *Tregoning and Watson*, 2009; *Tregoning et al.*, 2009]. We use the resulting 3D position time series derived from this "final

Table 1. GPS Processing Strategies

	Lo[a]	ST1[b]	ST2[b]	ST3[b]
Software	GIPSY-OASIS[c]	GAMIT 10.33 - GLOBK[d]	GAMIT 10.33 - GLOBK[d]	GAMIT 10.33 - GLOBK[d]
Station estimation	PPP with ambiguity resolution	Network resolution	Network resolution	Network resolution
Troposphere strategy				
Meteorological observations	Standard sea level model	Standard sea level model	Empirical global pressure and temperature model (GPT)[e]	Empirical global pressure and temperature model (GPT)[e]
Mapping Function	NMF[f]	NMF[f]	VMF1[g]	VMF1[g]
ZTD estimation	Constrained random walk[h]	Every 2 h	Every 2 h	Every 2 h
Atmospheric gradient	Random walk[h]	No	No	1 per session
Loading correction applied				
Oceanic	Yes	Yes	Yes	Yes
Atmospheric	No	No	Yes	Yes
Hydrologic (a posteriori correction)	No	No	No	Yes[i]
Reference frame ~ North America	Wrt MDO1	combination with a global solution	combination with a global solution	combination with a global solution

[a]Strategy code from *Lowry* [2006].
[b]Strategy code from this study.
[c]*Zumberge et al.* [1997].
[d]*Herring et al.* [2006].
[e]*Boehm et al.* [2007b].
[f]*Niell* [1996].
[g]*Boehm et al.* [2006b].
[h]*Bar-Sever et al.* [1998].
[i]Derived from GRACE data (see Appendix A for details).

climatic and loading" strategy (ST3, Table 1) in the following sections.

3.2. Comparison With Other GPS Position Time Series

[13] We performed a comparison between our time series and those used by *Lowry* [2006] to evaluate the tectonic signal to noise improvement. In Lowry's study, the GPS data were processed following the processing strategy of *Larson et al.* [2004] with the GIPSY-OASIS software package [*Lichten and Border*, 1987]. A summary of the strategy is presented in Table 1 and we refer the reader to *Larson et al.* [2004] for the details of their processing. There are several differences in our GPS analysis and that presented by *Lowry* [2006]. First, in our processing, the daily positions were estimated by inverting double differenced observations between all sites measured simultaneously whereas in the work of *Lowry* [2006] the station positions were estimated independently with a Precise Point Positioning strategy [*Zumberge et al.*, 1997]. Second, we used improved pressure and temperature models and tropospheric mapping functions based on data from numerical weather models that were not available at the time of the former study. Third, we corrected for the oceanic, atmospheric and hydrological loadings whereas the positions from *Lowry* [2006] were only corrected for ocean tide loading. Finally, we expressed our solution in the North American plate reference frame while *Lowry* [2006] calculated coordinates with respect to McDonald Observatory, Texas (MDO1), assumed to be on stable North America (the latter point explains why, on Figure A1, the inter-large-SSEs slopes from the two studies differ).

[14] As described previously, we determined the improvement of the coordinate estimates using equation (1), over the common "linear" inter-large-SSEs period (i.e., 2003.0 to 2005.0). The mean value of improvement of the repeatability is about 50% on the three components (Table A1 and Figure A1). Half, 90% and all of this improvement, on the north, east and vertical components respectively, are related to the network resolution relative to the PPP resolution (ST1 with respect to *Lowry* [2006]). The remaining improvement is due to the implementation of the "climatic and loading" strategy (ST2 or ST3). The noise level of the position time series in the current study is reduced by one half with respect to previous studies [*Kostoglodov et al.*, 2003; *Larson et al.*, 2004; *Franco et al.*, 2005; *Lowry*, 2006]. Our results are therefore better suited to analyze the 1997–2008 SSE succession in the Guerrero subduction zone.

4. Interpretation of the 1997–2008 Position Time Series

4.1. Periodic Signals in the Position Time Series

[15] We present 11 years of 3D GPS position time series derived from the ST3 strategy (Table 1) at 13 stations located in the Guerrero subduction zone and three stations located in the Oaxaca subduction zone (Figures 1, 2 and S2).[1] The daily position time series clearly show the three large, known SSEs on each of the three components in 1998, 2001–2002 and 2006 [*Lowry et al.*, 2001; *Kostoglodov et al.*, 2003;

[1]Auxiliary material for this paper is available in the HTML. doi:10.1029/2009JB006852.

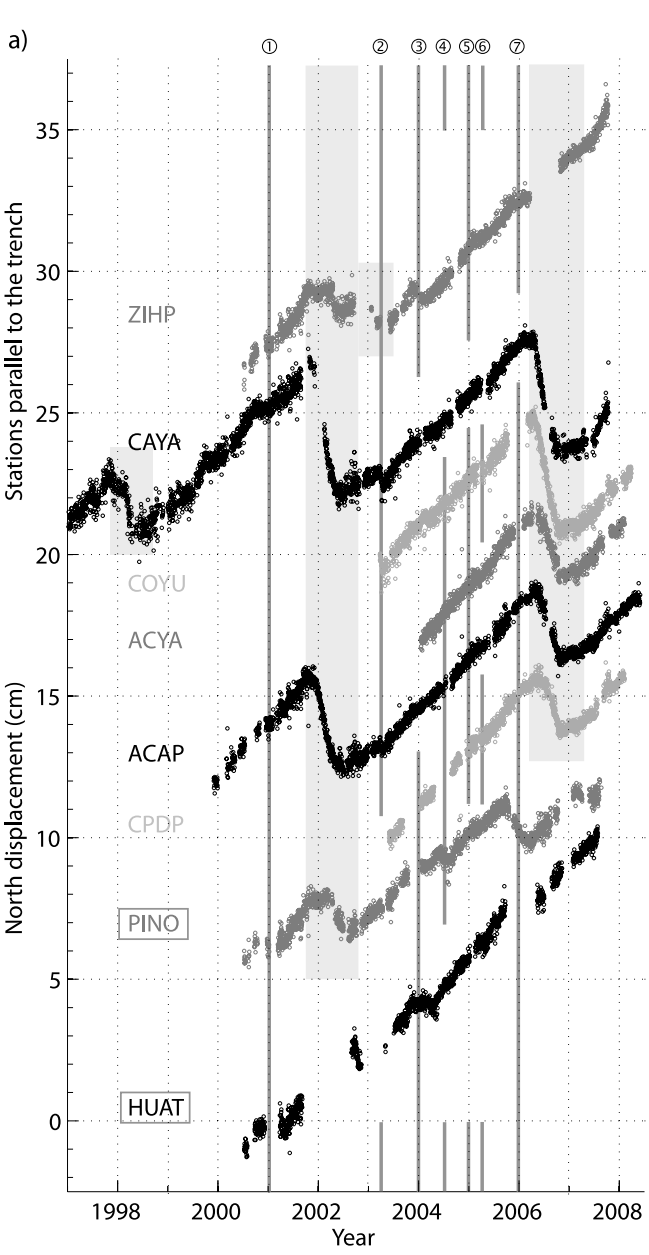

Figure 2. (a) North, (b) east, and (c) vertical position time series for the stations located on the parallel profile to the trench with respect to the North American plate reference frame. Position time series for the stations located on the perpendicular profile to the trench are presented in Figure S2. Scale is the same on Figures 2a, 2b, and 2c. Names of stations located in Oaxaca State are framed by a box. The large gray rectangles indicate the large 1998, 2001–2002 and 2006 SSEs. The width of these rectangles corresponds to the maximum duration of the SSEs over all the stations affected and all the GPS components. The vertical gray bars highlight the approximate median time of the detected small anomalous displacements that meet all the conditions and assumptions described in section 4.2. These bars are discontinuous. They only cross position time series on which an anomalous displacement was detected. The numbers on top of each graph identify the anomalous displacement events (AD) and correspond to the ADs in Table 2.

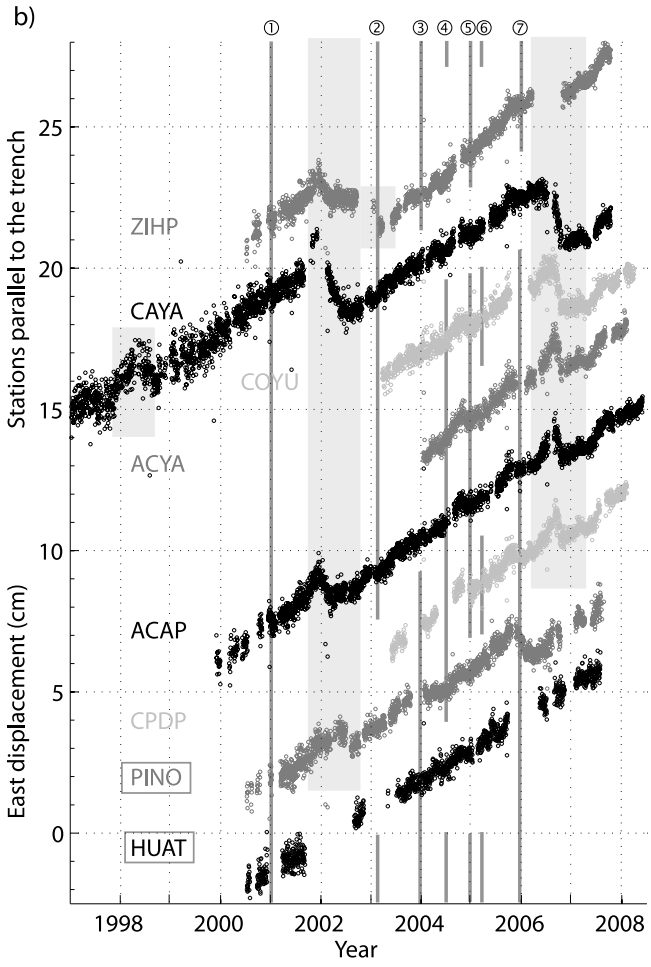

Figure 2. (continued)

Larson et al., 2004; *Lowry*, 2006; *Larson et al.*, 2007; *Brudzinski et al.*, 2007; *Correa-Mora et al.*, 2008; *Cotte et al.*, 2009] that are discussed in detail in section 5.

[16] Small annual periodic SSEs have been detected in the GPS time series of the stations located in Guerrero [*Lowry*, 2006] and in Central Oaxaca (at station OAXA, Figure 1) [*Brudzinski et al.*, 2007]. Based on a visual analysis of the GPS north component of our solution, it is no longer evident that small SSEs occurred annually between the large SSEs. Given that this horizontal component is roughly collinear with the convergence direction, anomalous displacements due to an SSE are expected to be mainly imprinted on this component (Figure 2a). Such anomalous displacements in the subduction zone of Guerrero should also be expressed in the vertical component; however, the vertical position time series are still too noisy to provide clear evidence of small annual SSEs (Figure 2c).

[17] We performed a spectral analysis, based on a Fourier transform, of the north, east and vertical position time series that cover at least 2 large SSEs (7 stations) to determine their frequency content (see Figure S1 for the details of the spectral analysis). The maximum amplitude of the spectrum for most of the stations corresponds to a period of 4 to 4.5 yrs (Figure S1), representing the period of occurrence of

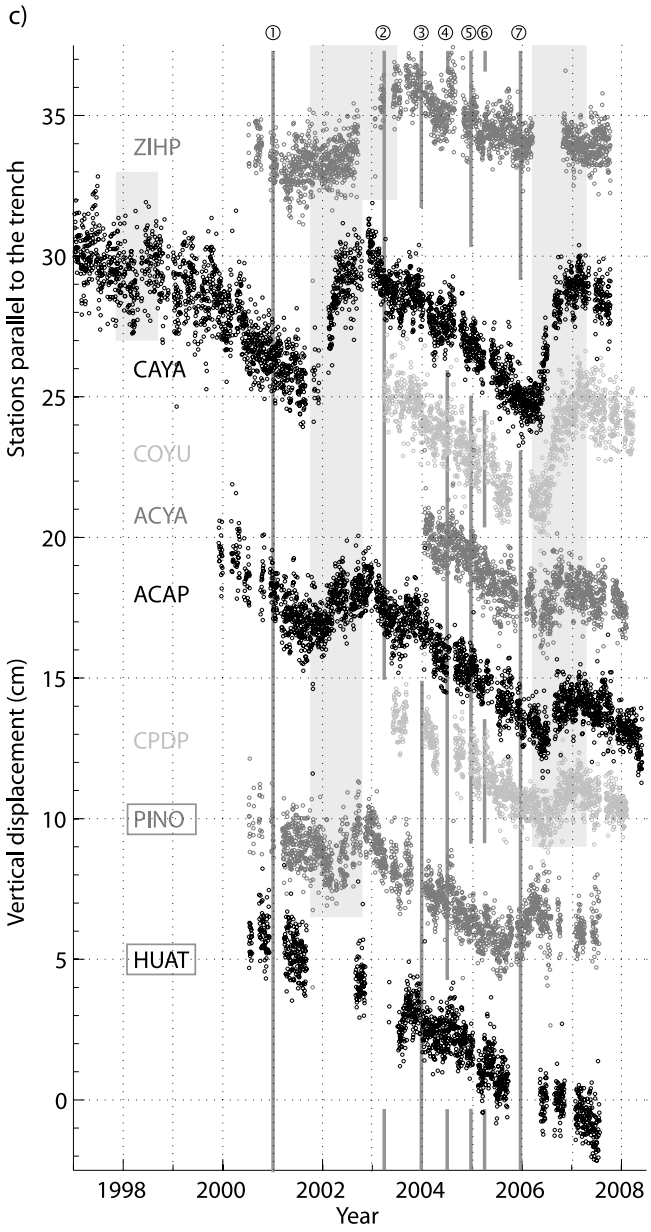

Figure 2. (continued)

the large SSEs [*Cotte et al.*, 2009]. Due to the small number of large SSEs observed with the GPS network, it is not yet possible to be more precise with this estimate. Equally, because the sawtooth function form of the signal is not perfectly repetitive and the time series are at most 11 years in length, it is still difficult to identify periodic signals at higher frequencies. Using this spectral analysis, we thus cannot corroborate previous observations of annual periodic SSEs.

4.2. Nonperiodic Signals in the Position Time Series

[18] Visually, some time series seem to be affected by small, non-periodic anomalous displacements (Figure 2). We implemented a tool that detects anomalous displacements automatically on the horizontal components (the vertical component remains too noisy for this analysis). We applied a linear interpolation to the position time series to fill the data gaps and then a low-pass filter with a cut-off wavelength of 200 days (see Figures S3 and S4 for the choice of the smoothing parameter). We calculated the instantaneous velocity and the root mean square of the square of the differences between the inter-large-SSEs velocity and the instantaneous velocity. We thus obtained horizontal velocity deviations from the inter-large-SSEs velocity with respect to time (Figure 3a). We defined a first threshold value as twice the standard deviation of the time series to detect the large SSEs. To detect smaller anomalies, we defined a second threshold value as the level of noise of the time series excluding the SSE periods. This amounts to twice the standard deviation of the time series excluding the SSE periods (Figure 3a).

[19] Figure 3b presents the results of this method at the station ACAP (Figure 1). The 2001–2002 and 2006 SSEs are well detected at ACAP, as well as at all the other sta-

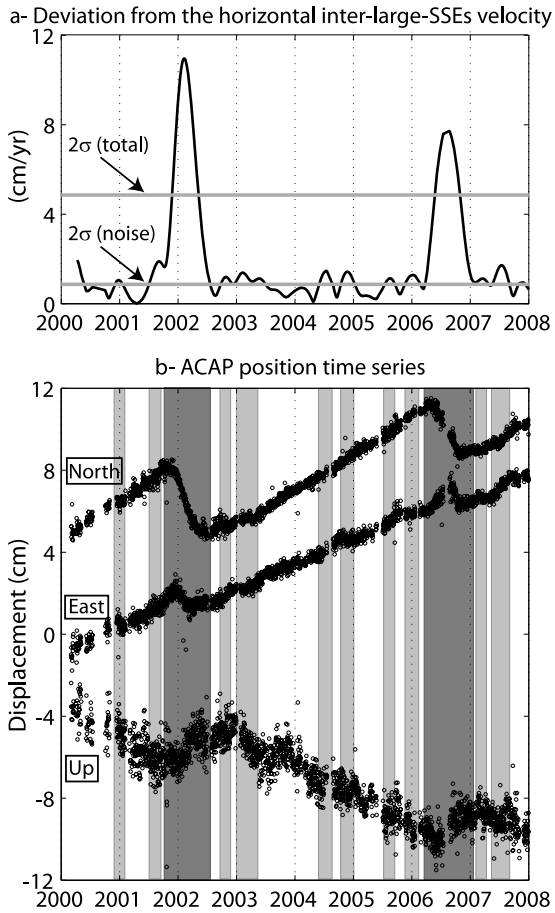

Figure 3. (a) Automatic detection of anomalous displacements with respect to the inter-large-SSEs trend. The time series of the horizontal velocity deviations from the inter-large-SSEs velocity at station ACAP is in black. The gray lines represent the threshold levels used to identify the large SSEs (2σ (total) line) and the small anomalous displacements (2σ (noise) line) (see section 4.2 for details). (b) North, east, and vertical position time series at station ACAP. The dark and light gray rectangles indicate the timing of the large SSEs and small anomalous displacements detected in Figure 3a, respectively.

Table 2. Description of the Small Anomalous Displacements That We Identified With the Automatic Detection Tool Described in Section 4.2.

AD[a]	n/N[b]	Affected Area	Δt[c]	t_m[d]	Comments
1	5/7	Guerrero (coast); Oaxaca (coast)	0.16–0.25; 0.41–0.5	2000.9; 2001.03	simultaneous start but early end for Guerrero stations in comparison to Oaxaca stations; start: 1.5 months earlier than in B07[e]; duration: twice as long at PINO than in L06[f]
2	6/10	Guerrero	~0.25	2003.13	start: later than in L06[f]
3	5/11	Oaxaca	~0.5	2004.1	start: 1 month earlier than in B07[e]; duration: more than twice as long than in B07[e]; no displacement at COYU and DOAR (horizontal displacement of 6 mm in B07[e])
4	6/12	Oaxaca - Guerrero	0.16–0.25	2004.5	maximum displacement at PINO; in Guerrero: smooth accelerations or decelerations of the instantaneous velocity
5	8/13	Guerrero	0.16–0.25	2005.0	all stations in Guerrero, except at CAYA; smooth variation on the north component; steep change in direction on the east component
6	5/13	Guerrero	0.08–0.16	2005.25	low amplitude; few Guerrero stations only; relatively low constraints
7	10/12	Oaxaca - Guerrero	0.41–0.5	2006.0	start: earlier at PINO than in Central Oaxaca (CM08[g]); duration: more than twice as long at PINO than at stations in Central Oaxaca (CM08[g])

[a]AD, anomalous displacement.
[b]n/N, number of stations affected with respect to the total number of stations operational at the date considered.
[c]Δt, maximum duration (in year).
[d]t_m, approximate median time.
[e]B07, *Brudzinski et al.* [2007].
[f]L06, *Lowry* [2006].
[g]CM08, *Correa-Mora et al.* [2008].

tions. Ten small anomalous displacements are detected at ACAP (Figure 3), but not at all the other stations. The small anomalous displacements might result from artifacts or noise in the processing. We thus define an SSE only when an anomalous displacement can be detected simultaneously at 4 or more GPS stations.

[20] We identify 7 small SSEs from 2001 to 2007 (Figure 2 and Table 2). The region affected by those 7 small anomalous displacements is not always the same. Stations located only in the Oaxaca State (HUAT, OAXA, PINO) or only in the Guerrero State sometimes recorded anomalous displacements (Table 2, AD 3 and AD 2, 5, 6, respectively). For the three other anomalous displacements, stations located both in the Oaxaca and Guerrero States were affected (Table 2, AD 1, 4 and 7).

[21] It is difficult to define accurately the timing of the anomalous displacements at each station because of data gaps. However, for each anomalous displacement, we determined the duration and the median time based on the best position time series. It seems that when the Oaxaca stations were affected by an anomalous displacement, the displacement lasted for roughly 5–6 months whereas when no slip was detected at these stations the displacement lasted for roughly 2–3 months at most.

[22] The anomalous displacements that we detected in 2004 and 2006 at the Oaxaca stations were observed by *Brudzinski et al.* [2007] and *Correa-Mora et al.* [2008], although with different timing and durations (Table 2). However, it has not been reported previously that some stations located in the Guerrero State were also affected during this period. For the first two anomalous displacements in 2004 (Table 2, AD 3, 4), the deformation at the Guerrero stations consist of smooth accelerations or decelerations of the instantaneous north and east velocities (Figures 2a and 2b). The anomalous displacements AD 5 and 7 (Table 2) consist mainly of a steep westward change of direction on the east component (Figure 2b).

[23] Finally, the amplitude of the anomalous displacements is not very well constrained but is usually of 5 mm or less at the Guerrero stations. The amplitude of displacement at the stations located in the Oaxaca State is higher during the first anomalous displacement (AD 1, Table 2, < 1 cm), as well as during the 2004 and 2006 SSEs [*Brudzinski et al.*, 2007; *Correa-Mora et al.*, 2008] but not very well constrained in this study because of data gaps (Figure 2).

4.3. Relation Between SSEs and Tremor Activity

[24] Non-volcanic tremor (NVT) activity has recently been observed in the Guerrero subduction zone [*Payero et al.*, 2008]. The authors built an approximate catalog of NVT activity (Figure 4) based on a visual examination of daily spectrograms at a few stations in the Guerrero region over the 2001–2007 period. More robust methods could not be applied on these data due to the limited number of stations that could be used on the 2001–2005 period. However, *Payero et al.* [2008] showed that highest NVT activity occurred during the large 2001–2002 and 2006 SSEs in Guerrero. Excluding the periods of these large SSEs, 4 peaks of NVT activity can be identified visually over the 2001–2005 period and three peaks over the 2005–2007 period (Figure 4). For this last group, we also used the information obtained after the application of a 60-day window average [*Payero et al.*, 2008, Figure S4]. The identification of these peaks is based on a qualitative method and few data; hence, it is a first attempt to compare the timing of the NVT activity with the timing of the small anomalous displacements described in the previous section.

[25] The peaks of NVT activity are not randomly distributed with respect to the timing of the small anomalous displacements. Six of the peaks roughly border the anoma-

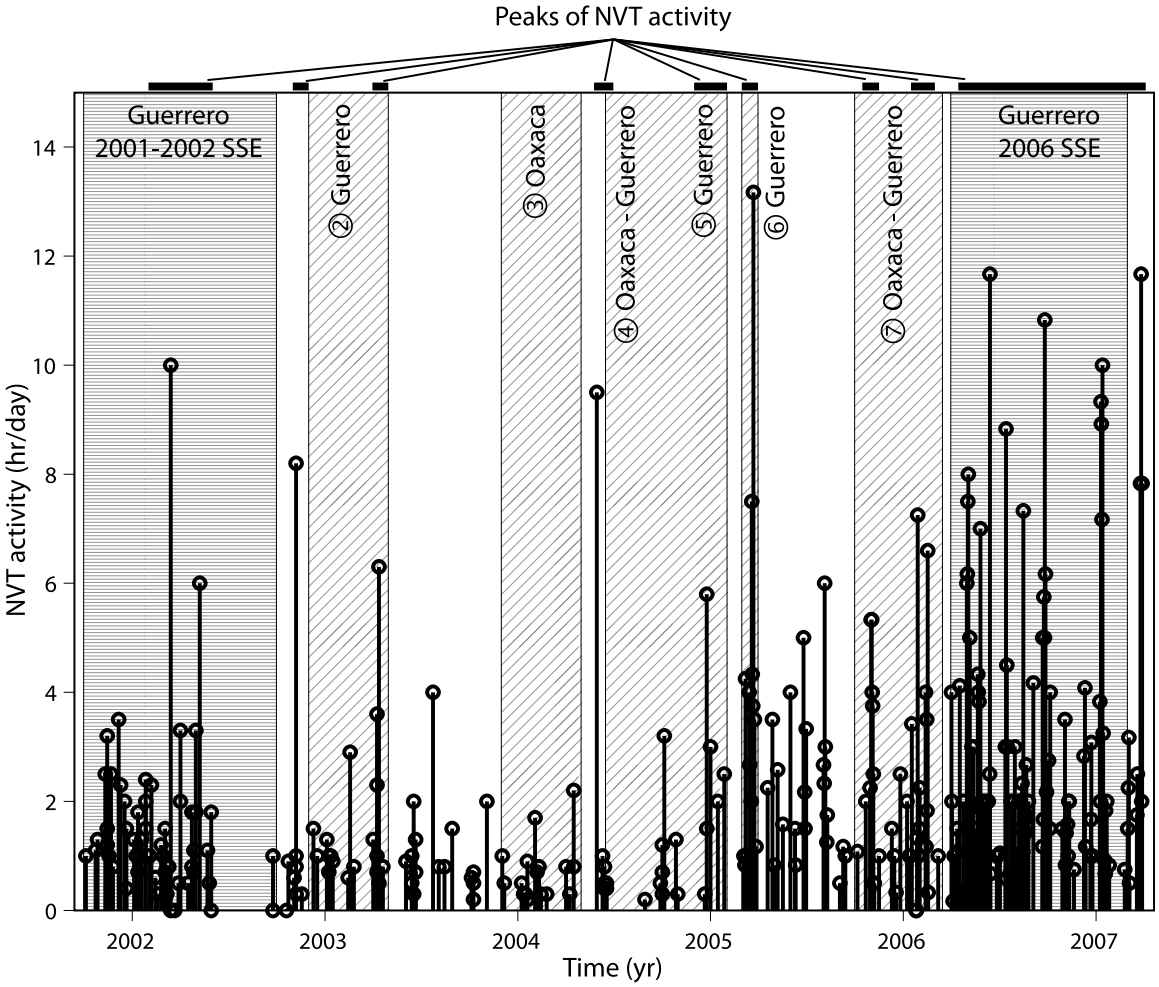

Figure 4. Comparison between the NVT activity (hours of tremor burst per day) in Guerrero with respect to time [from *Payero et al.*, 2008] and the time of occurrence of the anomalous displacements detected in this study (section 4.2). The times of the large 2001–2002 and 2006 SSEs are indicated with horizontal shading. The times of the small anomalous displacements, along with their label (see Table 2), are indicated with diagonal shading. The black lines at the top of the figure indicate the time of the NVT activity peaks.

lous displacements AD 2, AD 4 and 5, and AD 7 (Figure 4). The seventh peak occurs at the time of the anomalous displacement AD 6 (Figure 4). No peak is identified around the anomalous displacement AD 3. However, the GPS stations affected by this anomalous displacement are mainly located in the Oaxaca State whereas the seismological data used in the study of *Payero et al.* [2008] do not have the capacity to reveal NVT activity in this area. From the comparison of the timing of NVT and small anomalous displacements, we suggest that these two phenomena are apparently correlated in time in the Guerrero subduction zone. This observation supports the idea that the detected anomalous displacements are small SSEs.

5. The 2001–2002 and 2006 SSEs Characteristics

5.1. Method

[26] We analyzed the 2001–2002 and 2006 SSEs at each station that meets the following conditions: 1) the station must have at least two years of data outside the period of a large SSE, and 2) the station must have acquired data during the SSE. However, we made two exceptions: we kept the stations ZIHP and HUAT for the 2006 SSE analysis despite discontinuities in the data. Although it is not possible to recover the time evolution of the surface displacement at these stations during the SSE, the estimate of cumulative displacement is possible and the presumed timing roughly corresponds to that of the nearest stations (Figure 2).

[27] We applied a linear interpolation to the position time series to fill the data gaps and then a median filter with a sliding window of 30 days. We then subtracted the steady inter-large-SSEs velocity from each position time series. The cumulative displacement during the SSE was calculated as the displacement between two successive zero-slope portions of the position time series. The associated error is the quadratic sum of the standard deviations of the zero-slope before the SSE and after the SSE. To determine the displacement time evolution, we averaged the site position over

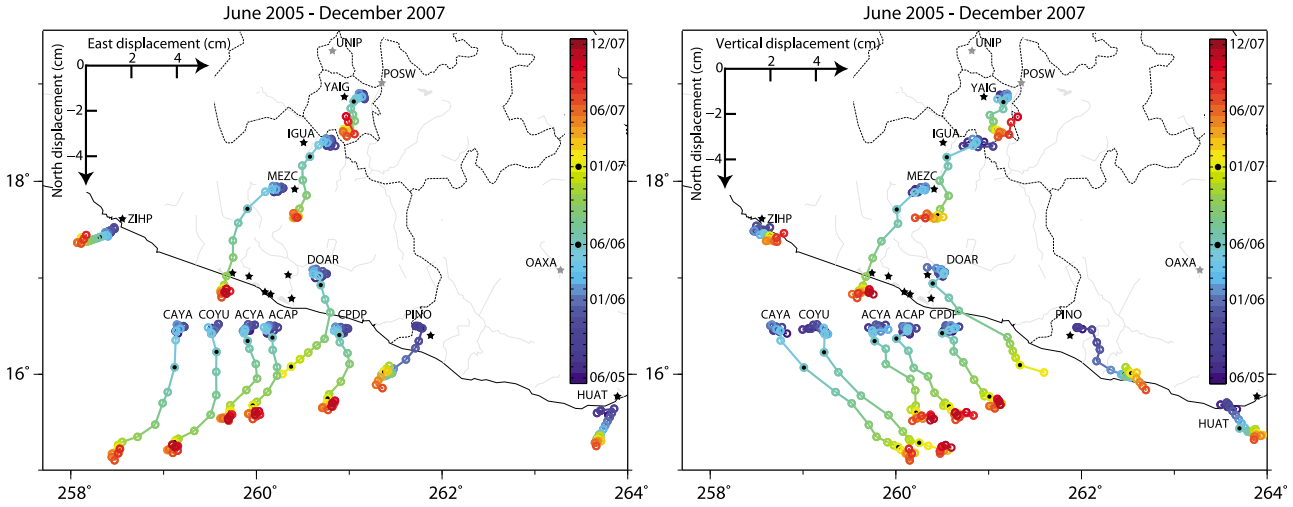

Figure 5. 3D time evolution of the displacement at each analyzed station from June 2005 to December 2007 representative of the 2006 SSE (see text for explanation, section 5.1). (left) Monthly cumulative displacement (in cm) with respect to the north and east components. (right) Monthly cumulative displacement (in cm) with respect to the north and vertical components. The displacement curves, for the close coastal GPS sites, are not plotted exactly at the GPS site location, but are aligned to allow a rapid comparison of the temporal evolution of the displacement at these sites. The inter-large-SSEs velocity has been removed from the motion of each station. The displacement at each site before and after the SSE is indicative of the noise on the cumulative monthly displacement determination on each component. The color bar indicates the time (month/year). Similar representation for the 2001–2002 SSE is provided in the auxiliary material (Figure S5).

10 days around the 1st of each month and plotted the monthly cumulative displacement. Figures 5 and S5 represent the 3D time evolution of the displacement at each analyzed station for both events. Figure 6 shows the horizontal and vertical cumulative surface displacements for both events. Figures 5, 6, and S5 show that there are roughly twice as many stations available to analyze the spatiotemporal evolution of the surface displacement for the 2006 SSE than for the 2001–2002 SSE. We therefore first describe the spatiotemporal evolution of the 2006 SSE displacement.

5.2. Spatiotemporal Evolution of the 2006 SSE Surface Displacement

[28] Before the start of the 2006 Guerrero SSE, an anomalous displacement at PINO occurred from mid-September/October 2005 to mid-March 2006 (Figures 2 and 5). Despite the data gap in the 3D position time series at HUAT, the lower and upper bounds for the timing of the event can be determined and coincide with the finding at PINO. The anomalous displacement in Oaxaca over at most 5–6 months had ended before the beginning of SSE displacement at the closest station in the Guerrero State (i.e., CPDP, Figure 1). This result is slightly different from that of *Brudzinski et al.* [2007] and *Correa-Mora et al.* [2008] for stations located in central Oaxaca. According to these studies, the anomalous displacement began in central Oaxaca in early 2006, three months later than at station PINO, and ended around April 2006. The duration of the event is therefore twice as long at PINO according to our observations.

[29] The anomalous SSE displacement at Guerrero stations lasted from 5 to 11 months depending on the location of the station (black markers are for the 1st of June 2006 and 1st of January 2007 on Figure 5). The initiation of the event was spread between stations over two months. It began in April 2006 at the station CAYA located on the coast, in the middle of the NW Guerrero seismic gap, and then propagated southeastward along the coast and inland toward the northeast. The propagation was faster toward locations inland (~3.9 km/day) than along the coast and roughly parallel to the trench (1.2 km/day). The cessation of the SSE displacement was much more dispersed temporally among the GPS stations and occurred over 4 months, ending first at the three stations inland in November 2006, and lastly at COYU and CAYA, on the coast, at the end of February 2007 (Figures 1 and 5). These results confirm the first observations and assumptions made by *Larson et al.* (2007) in detailing the start of the event at each station and, particularly, in determining the end of the event in February 2007.

[30] Despite the noise in the monthly averaged cumulative displacement time series (Figure 5), three different phases can be distinguished in the time series. In the first two months (Figure 5), the change of direction of the displacement was very strong in the north component with respect to the inter-large-SSEs displacement direction whereas it was very subtle or non-existent in the east and vertical components. This observation relates to the stations located about 80 km away from the trench, but not the stations located further inland (MEZC, IGUA, YAIG).

[31] The 2nd phase was the longest and clearest phase and was shown by *Larson et al.* [2007, Figure 1]. In this phase, the horizontal displacements at the stations located on the coast evolved from a southeastward displacement to a southwestward displacement, with a very similar displacement pattern at stations ACYA, ACAP, DOAR, and CPDP

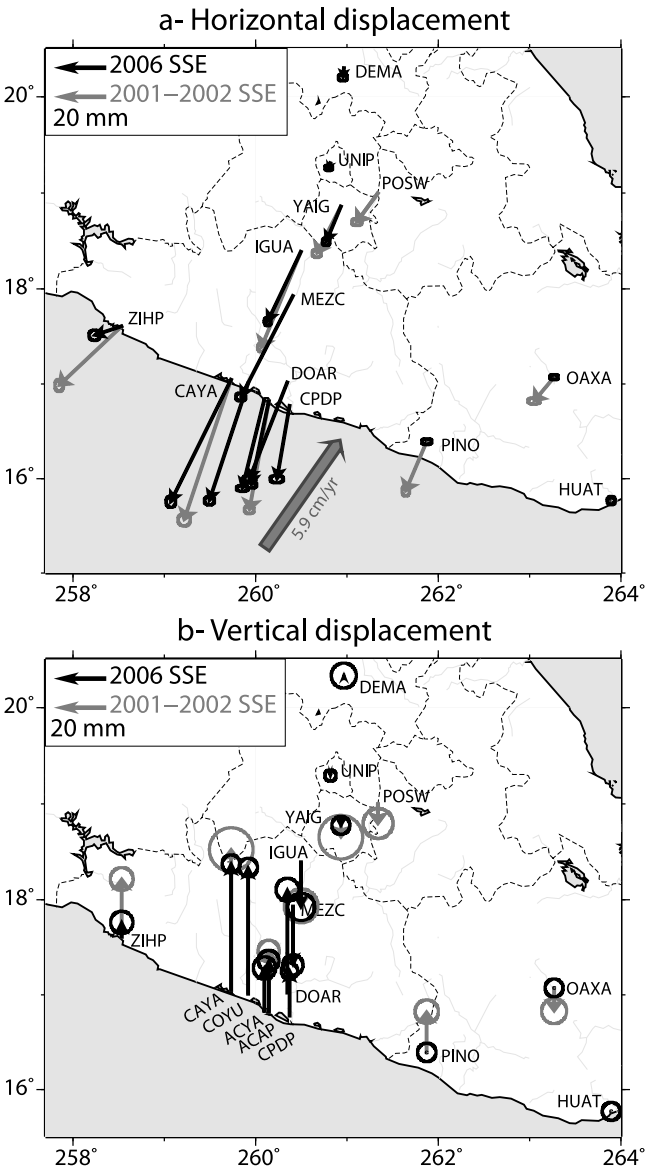

Figure 6. (a) Horizontal and (b) vertical cumulative displacements for the 2001–2002 and 2006 SSEs in gray and black, respectively. Ellipses are 95% confidence level. The large gray arrow indicates the direction and magnitude of NUVEL1-A relative plate motion between the Cocos and North American plates [*DeMets et al.*, 1994].

(Figure 5). However, the horizontal displacement evolved from southwestward to south at stations located inland. The vertical trend during this period was roughly linear at all stations but the inland stations moved downward whereas the coastal stations moved upward. These observations of horizontal and vertical direction change are of critical importance to locate the slip on the subduction interface in temporal slip inversions [*Radiguet et al.*, 2009].

[32] Finally, the 3rd phase can be detected only when analyzing also the vertical component of the displacement. It was shorter than the 2nd phase, and affected mostly the coastal stations. During this last phase that began in November 2006, the displacement on the east component stopped, the displacement on the north component continued but slowed down significantly and the displacement on the vertical component continued for 3–4 months (Figure 5). The observation of this last phase explains why we propose that the event stopped at the end of February 2007 rather than at the end of 2006 as suggested by *Larson et al.* [2007] and *Correa-Mora et al.* [2009].

[33] We detected three different phases characterizing the time evolution of the displacement at each site and two different time evolution patterns in space. On one hand, the displacement at the coastal stations is extremely complex with at least 3 phases: An initiation phase in which the south displacement prevails at slow rate, the main phase in which the displacement is different from the inter-large-SSEs motion on all the three components simultaneously, and the ending phase in which the east-west motion returns to steady state while the displacement on the north and vertical directions continues in the slow slip event sense at slow rate. On the other hand, the displacement at the inland stations, beyond the transition between the interseismic locked and freely slipping areas on the subduction interface, can be described mostly with the 2nd phase where all three components are active. Moreover, this main phase can be subdivided depending on the displacement direction evolution and also the displacement velocity evolution (slow-fast-slow, Figure 5). It lasted 5–7 months at all stations while the initiation and ending phases lasted about 2 and 3 months, respectively. Not including the two bounding phases implies an error in the estimate of the total duration of ~40%.

5.3. Spatiotemporal Evolution of the 2001–2002 SSE Surface Displacement

[34] For the 2001–2002 SSE, the variation in duration with respect to the location of the stations was larger than for the 2006 SSE and the duration ranged from 4 to 15 months. The 2001–2002 SSE also affected a much larger area, at least from the station ZIHP in the northwest to the stations PINO and OAXA in the southeast (~400 km along the coast, Figures 1, 2 and S5). The duration was the shortest (4–6 months) at stations in the Oaxaca State far away from the maximum slipping area.

[35] Stations in central Guerrero were affected for 6 to 13 months and station ZIHP for 15 months. The data gap at the end of 2002 in the ZIHP position time series may distort the interpretation. However, even if the anomalous displacement at ZIHP is the sum of the displacements caused by 2 distinct SSEs the time to return to steady state during the inter-event period is probably short with respect to the 15 months. Hence, we assume that it reflects only one SSE with acceleration and deceleration phases. As already shown [*Franco et al.*, 2005], the anomalous displacement is first detected at the station CAYA (Figures 1 and S5). However, the date of start and the propagation slightly differ between our observation and that of *Franco et al.* [2005]. In particular, we agree about the onset of displacement at half of the stations (CAYA, October 2001; ACAP, November 2001; YAIG, December 2001; POSW, January 2002) but estimate different initiation times at the other half of the stations (ZIHP, January 2002; PINO, April 2002; IGUA, December 2001; OAXA, April 2002). The difference potentially originates from the way the SSE initiation is determined, using only the north component, the horizontal components or the 3D components. The difference in the result affects mainly

the derived propagation rate. We found roughly similar propagation rates from station CAYA to the northwest (1.5 km/day) and to the southeast (1.3 km/day) along the coast and a much faster propagation rate inland toward the northeast (3.0 km/day) than that of *Franco et al.* [2005].

[36] The start of the anomalous displacement at each station was almost simultaneous on the three components (Figure S5). At all stations the horizontal displacement direction did not change up to July 2002 and was oriented south-southwestward (except at CAYA and ACAP during the first month of slip, Figure S5). After July 2002, when previous results showed approximately the end of the anomalous displacement [*Kostoglodov et al.*, 2003; *Yoshioka et al.*, 2004; *Iglesias et al.*, 2004; *Franco et al.*, 2005], we detect a second phase of the displacement (green to orange shades on Figure S5). The displacement on the east direction stopped, the displacement on the north direction slowed and the displacement on the vertical component continued in the same sense at stations along the coast but potentially in the opposite direction at stations inland. All stations, coastal or inland, followed the same time evolution pattern during the 2002 SSE: A main phase lasted about 7 to 9 months and a 2nd phase, only visible in our refined GPS analysis, lasted about 2 to 4 months (20–30% of the total duration). This is in general agreement with the 2006 SSE.

6. Discussion and Conclusions

6.1. The 2002 and 2006 SSEs: Are They Similar?

[37] As suggested by *Larson et al.* [2007], the two large SSEs share some common characteristics. In particular in this analysis, we found that in both SSEs the total displacement is highest at station CAYA on the coast but that the displacement is also very large at stations inland (about 150 km far from the coast, e.g., MEZC, IGUA), as large as at stations ACYA, ACAP or CPDP located on the coast at the eastern limit of the NW Guerrero gap (Figure 6). Moreover, the first stations to be affected by the SSEs are also those where the SSE lasts the longest: Stations CAYA and COYU located on the coast, in the middle of the NW Guerrero seismic gap. Finally, the initiation of the SSE displacement follows the same pattern in both SSEs with similar propagation rates, twice as fast in the dip direction of the subduction as along the strike of the subduction (Figure 5).

[38] However, the 2006 SSE affects a much smaller area than the 2001–2002 SSE: The horizontal and vertical displacements at station ZIHP, northwest of the northwest limit of the Guerrero gap is at least 3 times smaller, while no displacement is detected at stations located in Oaxaca State. Moreover, the cumulative displacement at each station in central Guerrero is smaller during the 2006 SSE (about 20% smaller on the horizontal displacement, Figure 6) and the duration is shorter (about 2 months less). Finally, we showed that the time evolution of the displacement is much more complex during the 2006 SSE - irrespective of location - although the last, slow phase is well detected at the end of both events (Figure 5). These last observations constrain the time evolution of the slip on the subduction interface and may suggest different slip evolution patterns.

6.2. Is Aseismic Slip Intruding Into the Seismogenic Zone?

[39] Whether the aseismic slip intrudes into the Guerrero seismogenic zone is not yet well resolved. It is nevertheless critical to better constrain whether the SSEs in this area release a part of the elastic strain accumulated during the interseismic period or increase it in the seismogenic zone [*Thatcher*, 2001]. A complete slip inversion study is beyond the scope of this paper. However, we tested the possibility that the downdip part of the seismogenic zone slipped during the SSEs. We first identified the distribution of coupling on the interface during the inter-large-SSEs interval that best describes the observed inter-large-SSEs velocities. We then determined the slip distribution at depth that best explains the surface displacements during the 2001–2002 and 2006 SSEs and compared this with the inter-large-SSEs coupling distribution. We used a dislocation model in an elastic half-space [*Savage*, 1983] to predict the displacements of stations on a cross section perpendicular to the trench from a slip distribution at depth (Figures 1 and 7).

[40] With an average trench-to-coast distance of ~60 km, the coastal GPS stations are located above the seismogenic zone. Accurate 3D cumulative displacements on these sites are essential in order to constrain the upward limit of the aseismic slip on the interface, in particular in the seismogenic zone. For the 2001–2002 SSE, we find horizontal displacements that are on average 40% and 60% larger than those of *Yoshioka et al.* [2004] and *Kostoglodov et al.* [2003], respectively, but similar to those of *Iglesias et al.* [2004] (Figure 6). For the 2006 SSE, the horizontal displacements are in good agreement with those of *Larson et al.* [2007], but the vertical displacements differ significantly. Our results are 40% larger than those of *Larson et al.* [2007] for the stations located on the coast but 40% smaller for the inland sites.

[41] We implemented the subduction interface with the geometry derived from *Pérez-Campos et al.* [2008] (Figure 7). The first segment is connected to the trench passing in the upper, freely slipping zone of the subduction (segment 1, up to 10 km depth). The next five segments correspond to the assumed seismogenic zone (up to ~25 km depth, segments 2, 3, 4) and transition zone (segments 5 and 6) [*Larson et al.*, 2004]. The last segment is a long, freely slipping segment in the ductile part of the subduction zone (segment 7). Varying slip can be imposed on different segments of this interface.

[42] The best fitting model for the inter-large-SSEs displacement rates is presented on Figure 7a. The GPS observations imply that a high degree of coupling is required from 14 to 30 km on the steep part of the fault plane with partial coupling updip and on the flat part of the fault plane toward both freely sleeping segments (1 and 7).

[43] The best fitting model for the surface displacement during the 2006 SSE (Figure 7b) requires slip from 19 km to 30 km depth on segments 4, 5, and 6. The first point to note is that slip on segments 2 and 3, corresponding to the upper part of the seismogenic zone, is not required to explain the observed surface displacements. Slip is therefore heterogeneous throughout the seismogenic zone [e.g., *Suárez et al.*, 1990]. The second interesting result is that the slip distribution between the lower part of the seismogenic zone

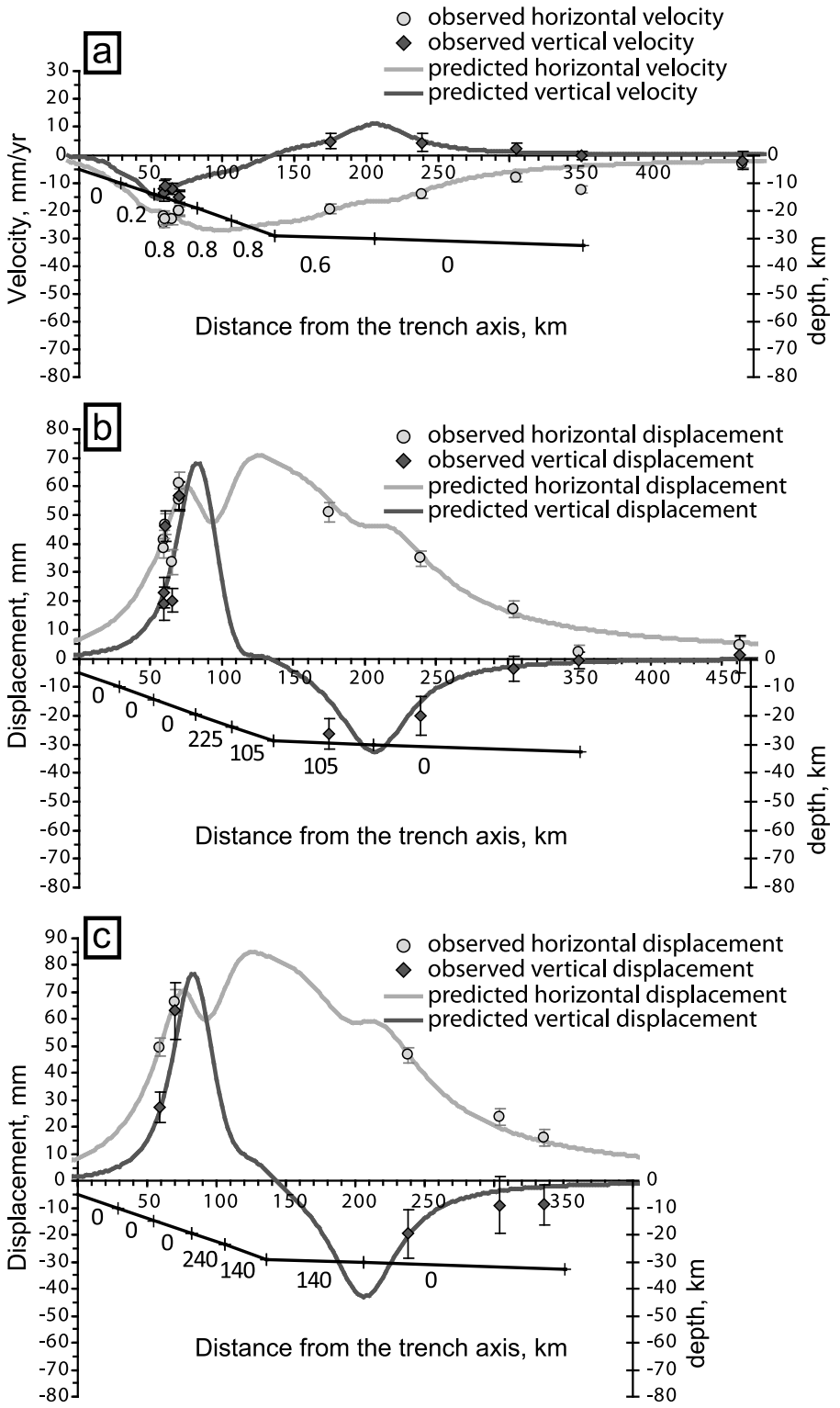

Figure 7. Dislocation models in an elastic half-space fitting (a) the 3D surface inter-large-SSEs velocity (coupling coefficients are annotated below the segments), (b, c) the 3D surface displacements during the 2006 and 2001–2002 SSEs, respectively (slip values, in mm, are annotated below the segments). The subduction interface is indicated by the black line, with crosses separating the different segments (1 to 7 from the trench). The 1st and 7th segments slip freely. Horizontal and vertical GPS observations used in the model (see Figure 1) are shown by circles and diamonds, respectively, with respect to the station's distance to the trench. Error bars are 95% confidence level. The light and dark gray curves depict the model predictions on the horizontal and vertical components, respectively.

(segment 4) and the transition zone (segments 5 and 6) is also heterogeneous. Taking into account the length of these segments, the equivalent moment magnitude released on the segments located on the steep part of the fault plane (segments 4 and 5) and on the segment located on the flat part of the fault plane (segment 6) would be equivalent.

[44] The analysis of the slip distribution at depth for the 2001–2002 SSE confirms that our simple model describes the major features of SSE in the Guerrero gap. Thus, the best fitting model (Figure 7c) has a similar slip pattern on the rupture plane as for the 2006 SSE, but with more slip on the three slipping segments. This result is qualitatively in good agreement with the equivalent moment magnitude calculated for both SSEs [e.g., *Franco et al.*, 2005; *Larson et al.*, 2007].

[45] In conclusion, this simple dislocation model shows that slip is required on the seismogenic zone (although not on the entire zone) to explain the observed surface displacements during both SSEs. This result contradicts *Correa-Mora et al.* [2009] who found that slip in the seismogenic zone (above 25 km) is not necessary to explain the motions of three sites in Guerrero (DOAR, COYU, CPDP). More complex slip inversion investigations will benefit from the new and more complete GPS observations presented here (vertical displacements at every station and refined horizontal displacements) to answer the question whether the SSE slip in Guerrero propagates into the seismogenic zone.

6.3. Behavior of the Guerrero and Oaxaca Subduction Segments

[46] The GPS time series analysis shows that 7 small anomalous displacements occurred in addition to the three large displacements related to the known SSEs. Two of the small anomalous displacements, AD 2 and 6, seem to have been produced by slow slip exclusively in the Guerrero area according to the currently available observations (Table 2 and Figure 2). The AD 2 event seems to be similar in spatial extension to the 2006 large SSE whereas the AD 6 event looks much more local or of very small magnitude.

[47] The anomaly found in 2000–2001 (AD 1, Table 2 and Figure 2) that began simultaneously on all the coastal stations from HUAT to ZIHP suggests that an SSE can occur over both the Guerrero and the Oaxaca segments simultaneously, at least in the shallow part of the subduction zone.

[48] Four of the anomalous displacements we identified (AD 3, 4, 5 and 7, Table 2 and Figure 2) are related to large SSEs that occurred in the adjacent Oaxaca subduction segment in 2004 and 2005–2006. This shows that the effect of slip on the subduction plane can be detected in GPS position time series at sites distant (>200 km) from the main slipping patch modeled by *Correa-Mora et al.* [2008, 2009].

[49] The SSE that *Correa-Mora et al.* [2008] modeled as the 2004 SSE began in early 2004 and continued up to October 2004 and encompassed both the first and second SSE that we found in 2004 (AD 3 and 4). Based on their data and our observations, we suggest that a significant part of the slip is localized deep on the subduction interface, in the first stage, to generate displacements at the inland Guerrero stations. The slip then propagated upward and westward toward PINO in the second and third stages. Indeed, large slip in the western part of the Oaxaca subduction plane should generate divergent slip vectors at stations located further west [*Cotton et al.*, 2008]. The small displacements we identified in the Guerrero area should help to identify more precisely the extension of the deep slip patch found by *Correa-Mora et al.* [2008] and the time evolution of the 2004 SSE.

[50] In our analysis, the 2005–2006 SSE (AD 7, Table 2), began a few months earlier in PINO located at the western limit of the Oaxaca subduction segment than in central Oaxaca [*Correa-Mora et al.*, 2008]. This new observation confirms the modeling result of *Correa-Mora et al.* [2009] that showed that the slip initiated in the western part of central Oaxaca, and should help to delineate the westward and upward limit of this slip patch. Moreover, simultaneously to the anomalous displacement at PINO, some anomalies were detected at most of the Guerrero stations, with mainly reversals of displacement on the east components. As for the 2004 anomalies, westward displacements in Guerrero would be generated by slip further east on the subduction interface.

[51] Finally, our analysis suggests that the initiation of the large 2006 SSE in central Guerrero appears to have been independent of the 2005–2006 SSE detected in Oaxaca. It thus confirms that the source regions of the 2006 Oaxaca SSE and 2006 Guerrero SSE may be distinct [*Correa-Mora et al.*, 2009].

[52] The analysis of 11 year GPS data in the Guerrero-Oaxaca subduction zone, complemented with results focused on the Oaxaca subduction zone [*Brudzinski et al.*, 2007; *Correa-Mora et al.*, 2008; *Correa-Mora et al.*, 2009], shows that there is no evidence of significant migration of the SSEs from one region to the other. The large SSEs may not trigger large SSEs in the adjacent region but can be detected at stations far from the main slipping patch. On the other hand, it cannot be excluded that sometimes the SSE may affect both regions simultaneously (e.g., in 2000–2001, AD 1, Table 2). Longer position time series are needed to confirm the repetition of such events.

6.4. Timing and Recurrence of the SSEs

[53] The correction for hydrological and atmospheric pressure loading in the analysis of the 1997–2008 GPS observations leads to a significant reduction of the non-tectonic noise in the position time series (about 50% on the three components) with respect to previously published time series. Hence, the SSEs are more evident - including several smaller events - and more precise timing of the events can be obtained. In particular, the use of the 3D displacements highlights the existence of initiation and ending phases. According to our results, the duration of the large 2001–2002 and 2006 SSEs is 30–40% longer than previously estimated [*Kostoglodov et al.*, 2003; *Franco et al.*, 2005; *Larson et al.*, 2007]. We found evidence for 7 small SSEs but do not find confirmation of the existence of annual periodic, small SSEs. This suggests that some of the previously identified signals [*Lowry*, 2006] may actually be artifacts of the earlier GPS processing strategy.

[54] Finally, despite the small number of observed large SSEs in Guerrero (currently only three), a 4–4.5 yr periodicity may be proposed. According to *Cotte et al.* [2009], if this recurrence time is reliable, the next SSE may occur in 2010. This hypothesis is a strong motivation to maintain the permanent GPS observation during future years. A densification of the network in critical places could also add crucial

information on a future event. To prepare the optimized observation of a future large SSE, we are (2009–2010) deploying additional GPS stations in Guerrero. We are also increasing the transmission speed of data where possible to monitor the onset of the next event in close to real time.

Appendix A: GPS Observations, GPS Processing Tests and Results

[55] The permanent GPS network "SSN-Sismologia-UNAM" (Figure 1) began in 1997 (see *Larson et al.* [2007] for details). By September 2008, data from 23 permanent stations were available, with 16 of these located in the Guerrero-Oaxaca zone (Figure 1). The configuration of the network in this zone is characterized by one trench-parallel transect along the coast, and one trench-perpendicular transect, linking Acapulco to the north of Mexico City. Four more sites (ZIHP, PINO, HUAT and OAXA) are located outside of these transects and are used to constrain the spatial extent of the SSE.

[56] We analyzed pseudorange and phase GPS data in single-day solutions using the GAMIT 10.33 software [*Herring et al.*, 2006] for the 16 Guerrero-Oaxaca continuous GPS stations (Figure 1) from 1997 to 2008. In order to decorrelate the tropospheric parameter estimation from the vertical positioning within the GPS processing, the GPS stations were included in a regional Mexican network with baselines longer than 500 km [*Tregoning et al.*, 1998; *Duan et al.*, 1996]. We solved for station coordinates, satellite state vectors, 13 tropospheric zenith delay parameters per site per day, and phase ambiguities using doubly differenced GPS phase measurements. We adjusted the a priori IGS final orbits and a priori IERS Earth orientation parameters in the processing. We followed IERS 2003 standards for modeling the solid earth tides, pole tides, and high frequency tide corrections [*McCarthy and Petit*, 2004], and used the IGS absolute antenna phase center model IGS_05.

[57] In our Mexican GPS analysis, we included a set of globally well distributed reference stations from the International GNSS Service (IGS) reference network [*Altamimi et al.*, 2007] to realize the reference frame. However, with the number of regional stations increasing over the 11 year period we analyzed, the number of globally distributed IGS stations included in our solution decreases (from 34 to 20) and becomes too small to achieve the reference frame stabilization. We thus combined our Mexican daily solutions with global daily solutions that we generated using the same analysis strategy. The reference frame was defined by minimizing the daily position deviations of IGS stations with respect to the North American plate reference frame while estimating a 7-parameter transformation. The height coordinates were down-weighted by a factor of 10 with respect to the horizontal components.

[58] Modeling the path delay in the troposphere is one of the main sources of error in GPS analysis. A common way to model the troposphere delay is to (1) model a priori the zenith total delay (ZTD) which is the sum of a hydrostatic (ZHD) and wet (ZWD) component; (2) compute the delay at any elevation angle using the corresponding mapping functions and (3) adjust the a priori delay in the least squares adjustment of the GPS observations to take into account its time-dependent variation. Recently, troposphere mapping functions [*Boehm and Schuh*, 2004; *Boehm et al.*, 2006a, 2006b, 2007a] and pressure and temperature models [*Boehm et al.*, 2007b] based on data from numerical weather models have been developed.

[59] In our standard ST1 solution (Table 1), we used the New Mapping Function (NMF) [*Niell*, 1996] and a priori ZHD derived from a standard sea level model for pressure and temperature (1013 hPa and 20°C at sea level), following the commonly used approach of many studies over the past decades. We did not estimate any atmospheric gradients. In the ST2 strategy (Table 1), we modeled the a priori ZTD by first deriving surface pressure estimates from the Global Pressure and Temperature model, GPT [*Boehm et al.*, 2007b]. Modeling more accurately the a priori ZHD generates changes in height estimates of up to 10 mm [e.g., *Tregoning and Herring*, 2006] and reduces significantly the annual variations in coordinate time series related to mismodeling of the ZHD [*Tregoning and Watson*, 2009]. In addition, in the ST2 analysis (Table 1) we used the Vienna Mapping Functions VMF1 [*Boehm et al.*, 2006b], where the coefficients of the hydrostatic and wet mapping function are determined from the ECMWF operational data analysis and are provided at 6-hourly intervals. The VMF1 reduces further the annual and semi-annual periodic variations related to deficiencies in the NMF and the Global Mapping Function (GMF) [*Boehm et al.*, 2007a] but also at higher frequencies [*Tregoning and Watson*, 2009]. Finally, we estimated one N-S and one E-W horizontal gradient per day in the ST2 strategy to estimate the azimuth-dependent part of the troposphere (Table 1).

[60] Correcting the GPS positioning for the effects of the oceanic, atmospheric and hydrological loadings is the second major issue in GPS processing dedicated to the observation of small tectonic displacements [*Blewitt et al.*, 2001; *Dong et al.*, 2002]. These loading deformations induce significant position variations at the several millimeter level on the vertical component with mainly semi-annual and annual periods for atmospheric and hydrological phenomena [e.g., *Dong et al.*, 2002] while sub-daily ocean loading effects alias to annual and semi-annual periods [*Penna and Stewart*, 2003; *Penna et al.*, 2007]. We applied, both in the ST1 and ST2 strategies, ocean tide loading corrections at the observation level (Table 1) using the FES2004 model [*Lyard et al.*, 2006]), a model that improves significantly the accuracy of the ocean tide prediction in coastal and continental shelf areas with respect to previous releases [*Vergnolle et al.*, 2008; *Melachroinos et al.*, 2008]. Correcting for the atmospheric loading is less common; however, atmospheric loading can induce sub-daily peak-to-peak vertical displacements of 4 to 18 mm for low to high latitude sites, respectively [*Tregoning and van Dam*, 2005]. In strategy ST2 (Table 1), we used crustal displacements predicted by convolving the National Centre for Environmental Prediction (NCEP) Reanalysis surface pressure estimates for the years 1997–2008 with elastic Green's functions [*Farrell*, 1972] to correct for the atmospheric loading at the observation level [*Tregoning and van Dam*, 2005].

[61] Finally, we corrected a posteriori for hydrological loading in the ST3 strategy. Hydrological loading can significantly affect the vertical displacements measured at GPS

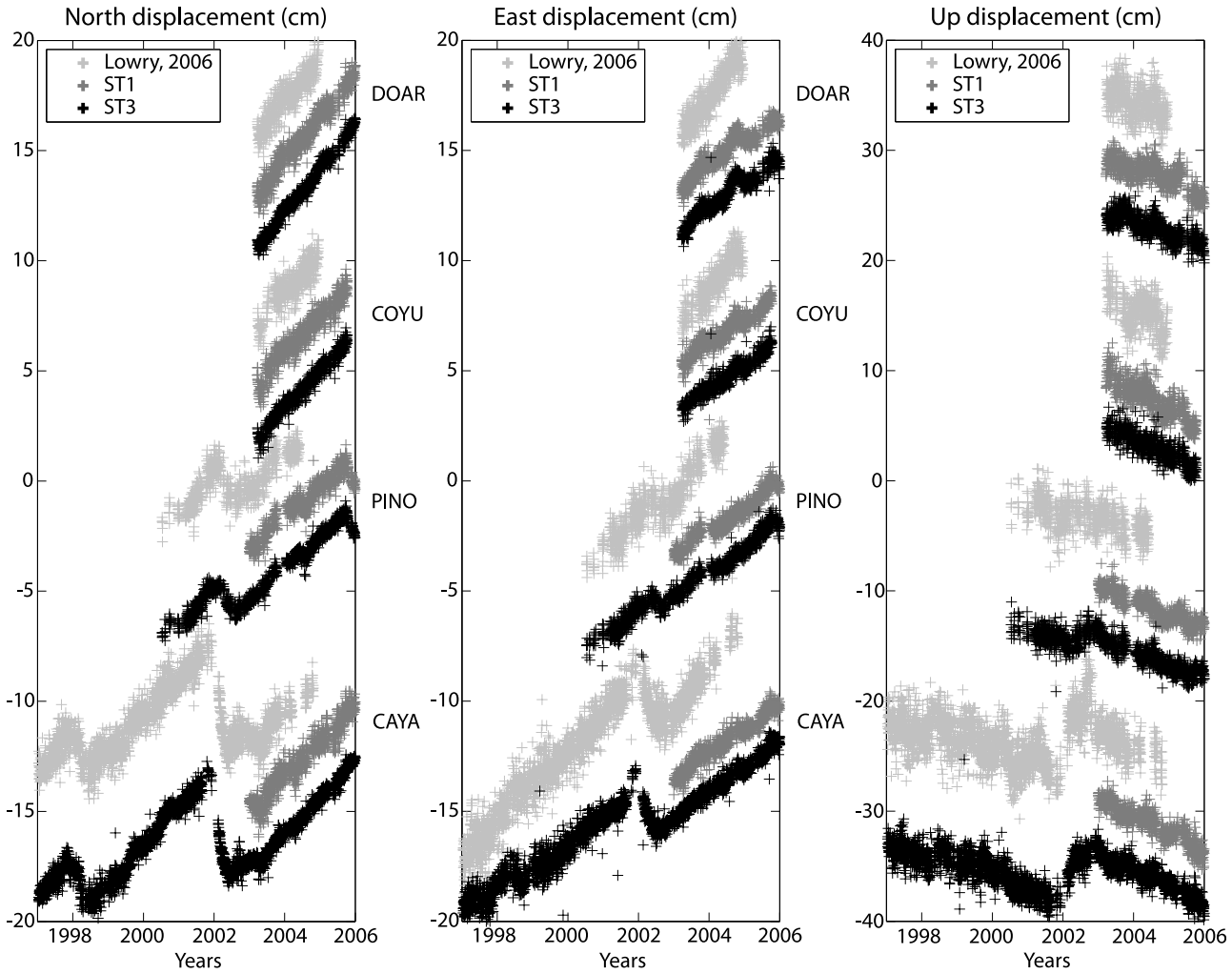

Figure A1. North, east and vertical position time series derived from the standard strategy (ST1, dark gray), the "final climatic and loading" strategy (ST3, black) and from *Lowry* [2006] (light gray). See text (section 3 and Appendix A) for details and Table 1 for the ST1, ST3 and *Lowry* [2006] strategy descriptions.

sites [e.g., *van Dam et al.*, 2001; *Tregoning et al.*, 2009] and can produce from 9 to 15 mm vertical displacements and millimeter horizontal displacements over many continental areas. High correlations have been found between horizontal and vertical position anomalies from GRACE and GPS in South America [e.g., *Davis et al.*, 2004; *Tregoning et al.*, 2009] and Europe [*Tregoning et al.*, 2009]. We removed a posteriori elastic deformation related to surface loading of hydrologic origin to reduce the annual perturbations that remained mainly in the vertical position time series (ST2 to ST3 solution, Table 1).

[62] We generated estimates of elastic deformation by characterizing changes in surface loads from gravity anomalies estimated from GRACE data following the method described by *Tregoning et al.* [2009]. We calculated gravity anomalies from the GRGS spherical harmonic fields by removing the mean of all estimates from 2002.6 to 2008. Assuming that the anomalies are caused entirely by changes in surface loads (i.e., of hydrologic origin), we converted the anomalies into surface load anomalies of equivalent water height for each epoch on a 1 by 1° global grid. We then convolved these temporal surface loads with Green's functions (using elastic load Love numbers) to generate the associated elastic deformation that would result at the GPS sites as a result of the surface loading [*Farrell*, 1972]. To extrapolate the observed surface loading time series from 2002.6 to 1997.0, we fitted these time series with an annual sinusoid of the form: $y(t) = A \sin(2\pi t + \varphi)$, where A and φ are the amplitude and phase of the annual hydrological loading deformation signal.

[63] We used the statistical parameters (weighted root mean square, wrms, mean value of the improvement, δ, equation (1)) described in section 3.1 and presented in Table A1 to evaluate the coordinate estimate improvement from one strategy to the other. Figure A1 shows the north, east and vertical position time series derived from ST1 and ST3 at 4 stations. The repeatability of the position time series derived from strategies ST1 and ST2 improves by a few to 30% (Table A1). As expected, the "first climatic and loading" GPS strategy, ST2, improves the vertical component with respect to the standard GPS strategy, ST1. Over 80% of the stations show smaller variability in the vertical component, with a mean value of improvement of 4.5%

Table A1. Mean Value of the Improvement in Percent (δ, Equation (1), Section 3.1) on the Three Components[a]

	ST1→ST2	ST2→ST3	Lo→ST1	Lo→ST3
N	12	12	8	8
North	31 (12)	1 (9)	23 (8)	50 (8)
East	2 (7)	2 (10)	47 (8)	53 (8)
Up	4.5 (10)	−0.5 (6)	46 (8)	46 (8)

[a]Value in parentheses (*n*) is the number of stations for which the wrms improved from one strategy to the next and *N* is the number of considered stations in the analysis. See text (section 3 and Appendix A) for details and Table 1 for the ST1, ST2, ST3 and Lo [*Lowry*, 2006] strategy descriptions.

(i.e., up to 1.3 mm, Table A1). Surprisingly, the north component is the most affected, with a mean value of improvement of ~30% (i.e., up to 1.4 mm). The level of improvement on the east component is much smaller with a mean value of improvement of 1.5% (up to 0.4 mm, Table A1). However, for the ST1 strategy, the wrms on the east component is 25% smaller than the wrms on the north component. The positive change of the statistical parameters, in our regional study, confirms the results of global studies on the necessity to use up-to-date and time varying mapping function and pressure models [*Tregoning and Herring*, 2006; *Boehm et al.*, 2007a], and to apply atmospheric loading corrections [*Tregoning and van Dam*, 2005; *Tregoning and Watson*, 2009] in order to obtain the most accurate coordinate estimates.

[64] The a posteriori global hydrologic loading correction, applied in the strategy ST3 (Table 1), shows statistically more subtle changes. We did not expect high changes on the horizontal components but 75% of the horizontal time series show a decrease in wrms (Table A1). In particular, the difference of wrms on the east component is statistically significant at 70% confidence for 5 of the 10 stations that have a lower wrms, but for only 2 sites at 90% confidence. Therefore, we suggest that hydrologic loading explains part of the remaining colored noise in the east component time series of the ST2 solutions. The result is more varied in the vertical component (Figure A2), and seasonal variations still remain in the ST3 position time series. Half of the final vertical ST3 position time series have a reduced wrms and the difference is statistically significant at 75% confidence for 5 of these 6 stations, but for only 4 at 90% confidence. For the other stations, the vertical repeatability deteriorates in the new analysis.

[65] We first made the assumption that the period on which we calculated the statistic (2003.0 to 2006.0) was free of SSE; hence, the statistical parameters were interpreted as noise around a linear trend. However, if small SSEs have occurred during this period as suggested by *Lowry* [2006] in the Guerrero subduction zone and by *Brudzinski et al.* [2007] in the Oaxaca subduction zone, removing the hydrological load could emphasize the reverse displacement during the small SSEs, which could then have increased the wrms. We analyzed qualitatively the changes between the ST2 and ST3 vertical position time series (Table 1) and compared these changes with the observations on the north component - the best determined component in this analysis and also where the displacements during large SSEs are the most obvious [e.g., *Kostoglodov et al.*, 2003; *Larson et al.*, 2007]. We found that removing the hydrological deformation signals removes anomalies at epochs 1997.5, 1999.5, and beginning of 2000, 2001, 2005, 2006, 2007 on most of the ver-

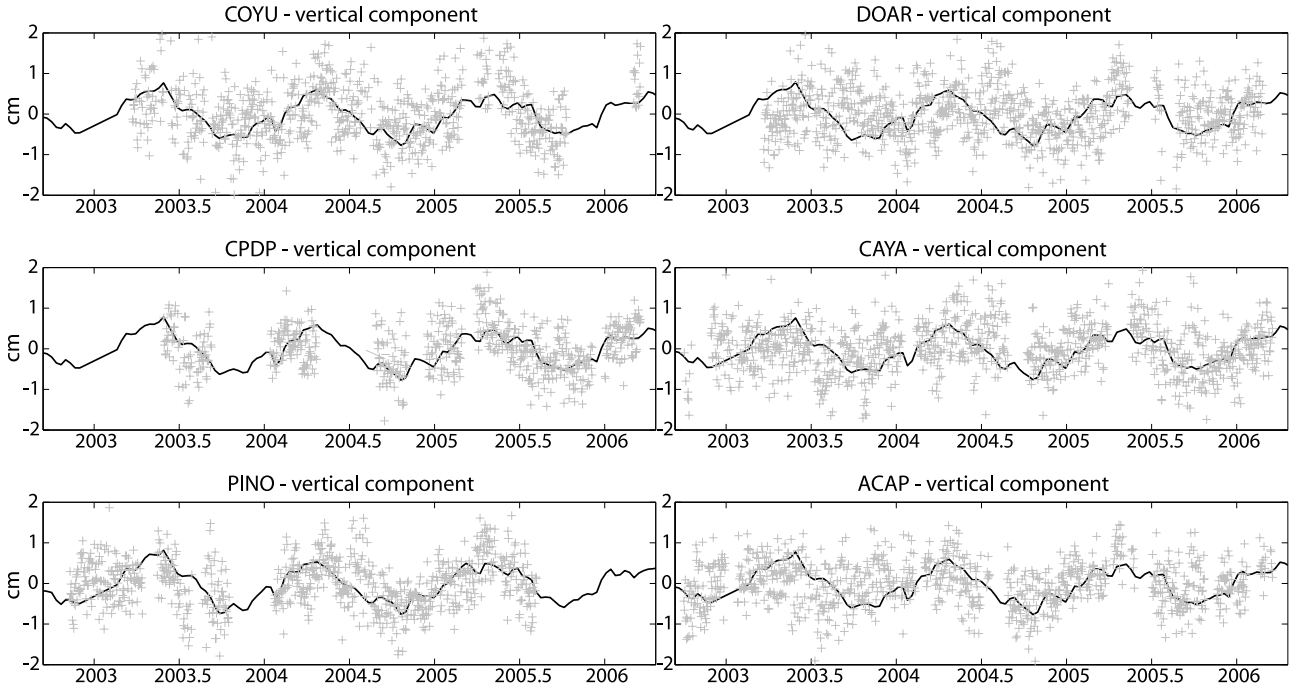

Figure A2. Vertical position time series derived from the "first climatic and loading" strategy (ST2, Table 1) overlaid with the observed vertical surface loading time series derived from the GRACE data (see Appendix A). The left-hand column shows sites where the wrms of the position estimates reduced when corrected for hydrological loading while on the right are sites where the wrms increased.

tical time series. Over these periods, the vertical time series become more linear, consistent with the north component. Anomalies are enhanced or shifted at the beginning of 2003 and 2005 at a few stations, which is also consistent with anomalous displacements seen in the north component of these stations. More details on these anomalous displacements are provided in section 4. Therefore, we consider that removing the hydrological loading improves the position time series.

[66] **Acknowledgments.** The GPS network maintenance and data acquisition were supported by Mexico's PAPIIT IN102105, IN103808 and CONACYT 46064 grants. We are grateful to all the people who participated in the GPS network maintenance. We acknowledge A.R. Lowry and K.M. Larson for providing us the GPS position time series published by *Lowry* [2006] and for fruitful discussions. We thank the Groupe de Recherche en Géodesie Spatiale for providing their GRACE solutions. We gratefully acknowledge the constructive reviews of the Associate Editor and an anonymous reviewer that significantly helped improve the original manuscript. This work has been supported by the French national programs Fluide-Faille-Flux (3F) from Institut National des Sciences de l'Univers/Centre National de Recherche Scientifique (INSU/CNRS), by the French national research agency (Agence Nationale de la Recherche, ANR G-GAP RA0000C069), by the French Scientific International Cooperation Program (PICS) and by the European Commission program Evaluation-Orientation de la Coopération Scientifique (ECOS-Nord).

References

Altamimi, Z., X. Collilieux, J. Legrand, B. Garayt, and C. Boucher (2007), ITRF2005: A new release of the International Terrestrial Reference Frame on time series of station positions and Earth Orientation Parameters, *J. Geophys. Res.*, *112*, B09401, doi:10.1029/2007JB004949.

Anderson, J. G., J. N. Brune, J. Prince, R. Quaas, S. K. Singh, D. Almora, P. Bodin, M. Oñate, R. Vasquez, and M. Velasco (1994), The Guerrero accelerograph network, *Geofis. Int.*, *33*, 341–371.

Bar-Sever, Y., P. M. Kroger, and J. A. Borjesson (1998), Estimating horizontal gradients of tropospheric path delay with a single GPS receiver, *J. Geophys. Res.*, *103*(B3), 5019–5036, doi:10.1029/97JB03534.

Blewitt, G., D. Lavallée, P. Clarke, and K. Nurutdinov (2001), A new global mode of Earth deformation: Seasonal cycle detected, *Science*, *294*, 2342–2345, doi:10.1126/science.1065328.

Boehm, J., and H. Schuh (2004), Vienna mapping functions in VLBI analyses, *Geophys. Res. Lett.*, *31*, L01603, doi:10.1029/2003GL018984.

Boehm, J., A. Niell, P. Tregoning, and H. Schuh (2006a), Global Mapping Function (GMF): A new empirical mapping function based on numerical weather model data, *Geophys. Res. Lett.*, *33*, L07304, doi:10.1029/2005GL025546.

Boehm, J., B. Werl, and H. Schuh (2006b), Troposphere mapping functions for GPS and very long baseline interferometry from European Centre for Medium-Range Weather Forecasts operational analysis data, *J. Geophys. Res.*, *111*, B02406, doi:10.1029/2005JB003629.

Boehm, J., P. J. Mendes Cerveira, H. Schuh, and P. Tregoning (2007a), The impact of mapping functions for the neutral atmosphere based on numerical weather models in GPS data analysis, *IAG Symop. Ser.*, vol. 130, edited by P. Tregoning and C. Rizos, pp. 837–843, Springer, New York.

Boehm, J., R. Heinkelmann, and H. Schuh (2007b), Short Note: A global model of pressure and temperature for geodetic applications, *J. Geod.*, *81*(6–8), 679–683, doi:10.1007/s00190-007-0135-3.

Brown, K. M., M. D. Tryon, H. R. DeShon, L. M. Dorman, and S. Y. Schwartz (2005), Correlated transient fluid pulsing and seismic tremor in the Costa Rica subduction zone, *Earth Planet. Sci. Lett.*, *238*, 189–203, doi:10.1016/j.epsl.2005.06.055.

Brudzinski, M., E. Cabral-Cano, F. Correa-Mora, C. DeMets, and B. Márquez-Azúa (2007), Slow slip transients along the Oaxaca subduction segment from 1993 to 2007, *Geophys. J. Int.*, *171*(2), 523–538, doi:10.1111/j.1365-246X.2007.03542.x.

Correa-Mora, F., C. DeMets, E. Cabral-Cano, O. Diaz-Molina, and B. Marquez-Azua (2008), Interplate coupling and transient slip along the subduction interface beneath Oaxaca, Mexico, *Geophys. J. Int.*, *175*, 269–290, doi:10.1111/j.1365-246X.2008.03910.x.

Correa-Mora, F., C. DeMets, E. Cabral-Cano, O. Diaz-Molina, and B. Marquez-Azua (2009), Transient deformation in southern Mexico in 2006 and 2007: Evidence for distinct deep-slip patches beneath Guerrero and Oaxaca, *Geochem. Geophys. Geosyst.*, *10*, Q02S12, doi:10.1029/2008GC002211.

Cotte, N., A. Walpersdorf, V. Kostoglodov, M. Vergnolle, J.-A. Santiago, I. Manighetti, and M. Campillo (2009), Anticipating the next large silent earthquake in Mexico, *Eos Trans. AGU*, *90*(21), 181–182, doi:10.1029/2009EO210002.

Cotton, F., M. Vergnolle, O. Thollon, M. Campillo, I. Manighetti, N. Cotte, A. Walpersdorf, V. Kostoglodov (2008), Comparison of slip distribution of large slow slip events in Guerrero subduction zone, *Eos Trans. AGU*, *89*(52), Fall Meet. Suppl., Abstract U33A-0039.

Davis, J. L., P. Elosegui, J. X. Mitrovica, and M. E. Tamisiea (2004), Climate-driven deformation of the solid Earth from GRACE and GPS, *Geophys. Res. Lett.*, *31*, L24605, doi:10.1029/2004GL021435.

DeMets, C., R. G. Gordon, D. F. Argus, and S. Stein (1994), Effect of recent revisions to the geomagnetic time-scale on estimate of current plate motions, *Geophys. Res. Lett.*, *21*, 2191–2194, doi:10.1029/94GL02118.

Dong, D., P. Fang, Y. Bock, M. K. Cheng, and S. Miyazaki (2002), Anatomy of apparent seasonal variations from GPS-derived site position time series, *J. Geophys. Res.*, *107*(B4), 2075, doi:10.1029/2001JB000573.

Doubre, C., and G. Peltzer (2007), Fluid-controlled faulting process in the Asal Rift, Djibouti, from 8-year radar interferometry observations, *Geology*, *35*(1), 69–72, doi:10.1130/G23022A.1.

Douglas, A., J. Beavan, L. Wallace, and J. Townend (2005), Slow slip on the northern Hikurangi subduction interface, New Zealand, *Geophys. Res. Lett.*, *32*, L16305, doi:10.1029/2005GL023607.

Dragert, H., K. Wang, and T. S. James (2001), A silent slip event on the deeper Cascadia subduction interface, *Science*, *292*, 1525–1528, doi:10.1126/science.1060152.

Duan, J., et al. (1996), GPS meteorology: Direct estimation of the absolute value of precipitable water, *J. Appl. Meteorol.*, *35*, 830–838, doi:10.1175/1520-0450(1996)035<0830:GMDEOT>2.0.CO;2.

Farrell, W. E. (1972), Deformation of the Earth by surface loads, *Rev. Geophys.*, *10*, 761–797, doi:10.1029/RG010i003p00761.

Franco, S. I., V. Kostoglodov, K. M. Larson, V. C. Manea, M. Manea, and J. A. Santiago (2005), Propagation of the 2001–2002 silent earthquake and intraplate coupling in the Oaxaca subduction zone, *Earth Planets Space*, *57*, 973–985.

Gwyther, R. L., C. H. Thurber, M. T. Gladwin, and M. Mee (2000), Seismic and aseismic observations of the 12th August 1998 San Juan Bautista, California, M5.3 earthquake, in *Proceedings of the 3rd Conference on Tectonic Problems of the San Andreas Fault System*, edited by G. Bokelmann and R. Kovach, Stanford Calif. Sch. of Earth Sci., Stanford Univ., Stanford, Calif.

Herring, T. A., R.W. King, S.C. McClusky (2006), Introduction to GAMIT/GLOBK, *Release 10.3*, Dep. of Earth Atmos. and Planet. Sci., Mass. Inst. of Technol., Cambridge, Mass., 28 Sept.

Hirose, H., K. Hirakara, F. Kimata, N. Fujii, and S. Miyazaki (1999), A slow thrust slip event following the two 1996 Hyuganada earthquakes beneath the Bungo Channel, southwest Japan, *Geophys. Res. Lett.*, *26*(21), 3237–3240, doi:10.1029/1999GL010999.

Iglesias, A., S. Singh, A. Lowry, M. Santoyo, V. Kostoglodov, K. M. Larson, S. I. Franco-Sanchez, and T. Mikumo (2004), The silent earthquake of 2004 in the Guerrero seismic gap, Mexico (M_w = 7.6), Inversion of slip on the plate interface and some implications, *Geofis. Int.*, *43*, 309–317.

Kostoglodov, V., W. Bandy, J. Dominguez, and M. Mena (1996), Gravity and seismicity over the Guerrero seismic gap, Mexico, *Geophys. Res. Lett.*, *23*(23), 3385–3388, doi:10.1029/96GL03159.

Kostoglodov, V., R. W. Valenzuela, A. Gorbatov, J. Mimiaga, S. I. Franco, J. A. Alvarado, and R. Peláez (2001), Deformation in the Guerrero seismic gap, Mexico, from leveling observations, *J. Geod.*, *75*(1), 19–32, doi:10.1007/s001900000144.

Kostoglodov, V., S. K. Singh, J. A. Santiago, S. I. Franco, K. M. Larson, A. R. Lowry, and R. Bilham (2003), A large silent earthquake in the Guerrero seismic gap, Mexico, *Geophys. Res. Lett.*, *30*(15), 1807, doi:10.1029/2003GL017219.

Larson, K. M., V. Kostoglodov, A. Lowry, W. Hutton, O. Sanchez, K. Hudnut, and G. Suárez (2004), Crustal deformation measurements in Guerrero, Mexico, *J. Geophys. Res.*, *109*, B04409, doi:10.1029/2003JB002843.

Larson, K. M., V. Kostoglodov, S. Miyazaki, and J.-A. Santiago (2007), The 2006 aseismic slow slip event in Guerrero, Mexico: New Results from GPS, *Geophys. Res. Lett.*, *34*, L13309, doi:10.1029/2007GL029912.

Lichten, S., and J. Border (1987), Strategies for high-precision Global Positioning System orbit determination, *J. Geophys. Res.*, *92*(B12), 12,751–12,762, doi:10.1029/JB092iB12p12751.

Linde, A. T., M. T. Gladwin, M. J. S. Johnston, R. L. Gwyther, and R. G. Bilham (1996), A slow earthquake sequence on the San Andreas fault, *Nature*, *383*, 65–68, doi:10.1038/383065a0.

Lowry, A. R. (2006), Resonant slow fault slip in subduction zones forced by climatic load stress, *Nature*, doi:10.1038/nature05055.

Lowry, A., K. M. Larson, V. Kostoglodov, and R. Bilham (2001), Transient slip in Guerrero, southern Mexico, *Geophys. Res. Lett.*, *28*, 3753–3756, doi:10.1029/2001GL013238.

Lyard, F., F. Lefevre, T. Letellier, and O. Francis (2006), Modelling the global ocean tides: A modern insight from FES2004, *Ocean Dyn.*, *56*, 394–415, doi:10.1007/s10236-006-0086-x.

McCarthy, D. D., and G. Petit (2004), IERS Conventions (2003), IERS Tech. Note 32, 127 pp., Verl. des Bundesamts für Kartogr. und Geod., Frankfurt am Main, Germany.

Melachroinos, S. A., et al. (2008), Ocean tide loading (OTL) displacements from global and local grids: Comparisons to GPS estimates over the shelf of Brittany, France, *J. Geod.*, *82*, 357–371, doi:10.1007/s00190-007-0185-6.

Miller, M. M., T. Melbourne, D. J. Johnson, and W. Q. Sumner (2002), Periodic slow earthquakes from the Cascadia subduction zone, *Science*, *295*, 2423, doi:10.1126/science.1071193.

Niell, A. E. (1996), Global mapping functions for the atmosphere delay at radio wavelengths, *J. Geophys. Res.*, *101*, 3227–3246, doi:10.1029/95JB03048.

Ohta, Y., J. Freymueller, S. Hreinsdóttir, and H. Suito (2006), A large slow slip event and the depth of the seismogenic zone in the south central Alaska subduction zone, Earth Planet. Sci. *Lett.*, *247*, 108–116, doi:10.1016/j.epsl.2006.05.013.

Ortiz, M., S. K. Singh, V. Kostoglodov, and J. Pacheco (2000), Constraint on the rupture areas of the Acapulco-San Marcos, Mexico earthquakes of the 1962(M 7.1;7.0) and 1957(M7.7), based on the analysis of tide records, *Geofis. Int.*, *39*, 337–348.

Ozawa, S., M. Murakami, and T. Tada (2001), Time-dependent inversion study of the slow thrust event in the Nankai trough subduction zone, southwestern Japan, *J. Geophys. Res.*, *106*(B1), 787–802, doi:10.1029/2000JB900317.

Pardo, M., and G. Suárez (1995), Shape of the subducted Rivera and Cocos plates in southern Mexico: Seismic and tectonic implications, *J. Geophys. Res.*, *100*(B7), 12,357–12,373, doi:10.1029/95JB00919.

Payero, J. S., V. Kostoglodov, N. Shapiro, T. Mikumo, A. Iglesias, X. Pérez-Campos, and R. W. Clayton (2008), Nonvolcanic tremor observed in the Mexican subduction zone, *Geophys. Res. Lett.*, *35*, L07305, doi:10.1029/2007GL032877.

Penna, N. T., and M. P. Stewart (2003), Aliased tidal signatures in continuous GPS height time series, *Geophys. Res. Lett.*, *30*(23), 2184, doi:10.1029/2003GL018828.

Penna, N. T., M. A. King, and M. P. Stewart (2007), GPS height time series: Short-period origins of spurious long-period signals, *J. Geophys. Res.*, *112*, B02402, doi:10.1029/2005JB004047.

Pérez-Campos, X., Y. Kim, A. Husker, P. M. Davis, R. W. Clayton, A. Iglesias, J. F. Pacheco, S. K. Singh, V. C. Manea, and M. Gurnis (2008), Horizontal subduction and truncation of the Cocos Plate beneath central Mexico, *Geophys. Res. Lett.*, *35*, L18303, doi:10.1029/2008GL035127.

Protti, M, V. González, T. Kato, T. Iinuma, S. Miyasaki, K. Obana, Y. Kaneda, P. LaFemina, T. Dixon, and S. Schwartz (2004), A creep event on the shallow interface of the Nicoya Peninsula, Costa Rica seismogenic zone, *Eos Trans. AGU*, *85*(47), Fall Meet. Suppl., Abstract S41D-07.

Radiguet, M., F. Cotton, M. Vergnolle, M. Campillo, V. Kostoglodov, N. Cotte (2009), Development of a new time-dependent slip inversion of Slow Slip Event: Application to the 2006 Guerrero SSE, *Eos Trans. AGU*, *90*(52), Fall Meet. Suppl., Abstract T11C-1829.

Reid, H. F. (1910), *The Mechanics of the Earthquake*, vol. 2, in *The California Earthquake of April 18, 1906*: *Report of the State Earthquake Investigation Commission*, edited by A. C. Lawson et al., 192 pp., Carnegie Inst. of Wash., Washington, D. C.

Sagiya, T. (2004), Interplate Coupling in the Kanto District, Central Japan, and the Boso Peninsula Silent Earthquake in May 1996, *Pure Appl. Geophys.*, *161*, 2327–2342, doi:10.1007/s00024-004-2566-6.

Savage, J. (1983), A dislocation model of strain accumulation and release at a subduction zone, *J. Geophys. Res.*, *88*(B6), 4984–4996, doi:10.1029/JB088iB06p04984.

Schwartz, S. Y., and J. M. Rokosky (2007), Slow slip events and seismic tremor at circum-Pacific subduction zones, *Rev. Geophys.*, *45*, RG3004, doi:10.1029/2006RG000208.

Singh, S. K., and M. Pardo (1993), Geometry of the Benioff zone and state of stress in the overriding plate in central Mexico, *Geophys. Res. Lett.*, *20* (14), 1483–1486, doi:10.1029/93GL01310.

Steigenberger, P., J. Boehm, and V. Tesmer (2009), Comparison of GMF/GPT with VMF1/ECMWF and implications for atmospheric loading, *J. Geod.*, doi:10.1007/s00190-009-0311-8.

Suárez, G., T. Monfret, G. Wittlinger, and C. David (1990), Geometry of subduction and depth of the seismogenic zone in the Guerero gap, Mexico, *Nature*, *345*, 336–338, doi:10.1038/345336a0.

Szeliga, W., T. I. Melbourne, M. M. Miller, and V. M. Santillan (2004), Southern Cascadia episodic slow earthquakes, *Geophys. Res. Lett.*, *31*, L16602, doi:10.1029/2004GL020824.

Thatcher, W. (2001), Silent slip on the Cascadia Subduction Interface, *Science*, *292*, 1495–1496, doi:10.1126/science.1061770.

Tregoning, P., and T. A. Herring (2006), Impact of a priori zenith hydrostatic delay errors on GPS estimates of station heights and zenith total delays, *Geophys. Res. Lett.*, *33*, L23303, doi:10.1029/2006GL027706.

Tregoning, P., and T. van Dam (2005), Atmospheric pressure loading corrections applied to GPS data at the observation level, *Geophys. Res. Lett.*, *32*, L22310, doi:10.1029/2005GL024104.

Tregoning, P., and C. Watson (2009), Atmospheric effects and spurious signals in GPS analyses, *J. Geophys. Res.*, *114*, B09403, doi:10.1029/2009JB006344.

Tregoning, P., R. Boers, and D. O'Brien (1998), Accuracy of absolute precipitable water vapor estimates from GPS observations, *J. Geophys. Res.*, *103*(D22), 28,701–28,710, doi:10.1029/98JD02516.

Tregoning, P., C. Watson, G. Ramillien, H. McQueen, and J. Zhang (2009), Detecting hydrologic deformation from space, *Geophys. Res. Lett.*, *36*, L15401, doi:10.1029/2009GL038718.

van Dam, T., J. Whar, P. C. D. Milly, A. B. Shmakin, G. Blewitt, D. Lavallée, and K. M. Larson (2001), Crustal displacements due to continental water loading, *Geophys. Res. Lett.*, *28*(4), 651–654, doi:10.1029/2000GL012120.

Vergnolle, M., M.-N. Bouin, L. Morel, F. Masson, S. Durand, J. Nicolas, and S. A. Melachroinos (2008), GPS estimates of ocean tide loading in NW-France: Determination of ocean tide loading constituents and comparison with a recent ocean tide model, *Geophys. J. Int.*, *173*, 444–458, doi:10.1111/j.1365-246X.2008.03734.x.

Yoshioka, S., T. Mikumo, V. Kostoglodov, K. M. Larson, A. Lowry, and S. K. Singh (2004), Interplate coupling and a recent aseismic slow slip event in the Guerrero seismic gap of the Mexican subduction zone, as deduced from GPS data inversion using a Bayesian information criterion, *Phys. Earth Planet. Inter.*, *146*, 513–530, doi:10.1016/j.pepi.2004.05.006.

Zumberge, J., M. Heflin, D. Jefferson, M. Watkins, and F. Webb (1997), Precise point positioning for the efficient and robust analysis of GPS data from large networks, *J. Geophys. Res.*, *102*, 5005–5018, doi:10.1029/96JB03860.

N. Cotte, M. Vergnolle, and A. Walpersdorf, Laboratoire de Géophysique Interne et Tectonophysique, CNRS, Observatoire de Grenoble, Université Joseph Fourier, BP53, F-38041 Grenoble, France. (mathilde.vergnolle@geoazur.unice.fr)

S. I. Franco, Servicio Sismológico Nacional, Instituto de Geofísica, Universidad Nacional Autónoma de México, Ciudad Universitaria, 04510 México, D.F., Mexico.

V. Kostoglodov and J. A. Santiago, Instituto de Geofísica, Universidad Nacional Autónoma de México, Mexico, Ciudad Universitaria, 04510 México, D.F., Mexico.

P. Tregoning, Research School of Earth Sciences, Australian National University, Canberra, ACT 0200, Australia.